Air Quality, Atmosphere & Health (2026) 19:178
https://doi.org/10.1007/s11869-026-02059-5

Network study of particulate matter distribution within the urban canopy layer using magnetic biomonitoring – assessing of CAR-FMI model performance and representativeness of a monitoring station

Jukka Limo[1] · Mari Kauhaniemi[2] · Leena Kangas[2] · Petriina Paturi[3] · Joni Mäkinen[1] · Ari Karppinen[2]

Received: 28 January 2026 / Accepted: 13 July 2026

Abstract

The distribution of air pollution in urban environments is greatly influenced by its source and the complexity of the urban environment, which determine the pollution concentrations in individual locations. Traffic is one of the main pollution sources in cities and, especially particulate matter (PM) poses a serious risk for public health. This study applies magnetic biomonitoring using moss bags to establish an extensive urban canopy layer monitoring network ($n=52$) to study the distributions and concentrations of magnetic PM. Moss bags were placed at street and roof levels within the grid plan area of Turku, Finland, for 62 days in late autumn. Samples were analysed for mass-specific magnetic susceptibility (χ), hysteresis parameters and elemental components. At street level, traffic was the primary source of magnetic PM and related elements. At higher altitudes, these concentrations were reduced and mainly replaced by crustal elements. Magnetic measurements were also applied to test for equivalence with the CAR-FMI dispersion model and to assess the representativeness of an air quality monitoring station in the city centre. Inconsistencies were observed between the model and magnetic PM concentrations at street level. At rooftop level, the model estimates were higher than indicated by the magnetic PM. The magnetic measurements complemented measurements derived from supplementary monitoring sensors and Turku monitoring station. The representativeness of the monitoring station should be re-evaluated, and recategorizing should be considered. Magnetic biomonitoring using moss bags is an unparalleled tool for monitoring airborne PM pollution and a reliable tool for evaluating monitoring stations and dispersion model performance.

Keywords Air quality · Magnetic particles · Urban pollution · Moss bag · Environmental magnetism

Introduction

The urban atmosphere is exposed to a variety of air pollutants, of which traffic-related airborne particulate matter (PM) and especially the fine particulates ($PM_{2.5}$) pose a serious global health risk. The coarse fraction of PM ($PM_{2.5–10}$) is less penetrative through the respiratory system but is still proven to be harmful to human health (Kim et al. 2018). In addition, the harmfulness of PM is enhanced by the ability of the magnetic PM fraction to incorporate toxic heavy metals into its structure (Yang et al. 2010). $PM_{2.5}$ is commonly associated with increased human respiratory and cardiovascular diseases, which in turn contributes to higher global morbidity and mortality rates (Soares et al. 2023). Recent studies have shown that $PM_{2.5}$ itself may even contribute neurodegenerative diseases (Cristaldi et al. 2022), and some studies suggest that PM-related heavy metals may accumulate in the human brain (Potter et al. 2021).

The health impacts of PM pollution are relevant because in the EU alone approximately 74% of the population lives in urban areas (EEA, 2019) and in 2018 about 74% of the population was exposed to concentrations of fine particulate matter ($PM_{2.5}$) above the WHO air quality guidelines (EEA, 2022). WHO has updated its health-based global air quality

✉ Jukka Limo
jukka.limo@utu.fi

[1] Department of Geography and Geology, University of Turku, Turku FI-20014, Finland

[2] Finnish Meteorological Institute (FMI), Helsinki 00101, Finland

[3] Department of Physics and Astronomy, University of Turku, Turku FI-20014, Finland

Published online: 06 August 2026

guidelines (WHO, 2021) and, as a result, in 2021 a substantial 97% of the urban population in the EU was exposed to concentrations of $PM_{2.5}$ above the new, stricter WHO air quality guidelines (EEA, 2023). In addition, the recently adopted EU Directive sets forward new limit values for the protection of human health to be attained by 1 January 2030 (EU, 2024).

The traffic related urban PM is released into the air as exhaust and non-exhaust emissions (Hueglin et al. 2005; Ketzel et al. 2007). The combustion process of gasoline and diesel engines release exhaust particles, while non-exhaust particles may have a more complex origin in the form of corrosion and mechanical wear of vehicle parts or road erosion (Beddows and Harrison 2021; Järlskog et al. 2022). As a result of its formation processes, urban PM therefore contains iron oxides, and the most common ferrimagnetic mineral is magnetite (Fe_3O_4) (Matzka and Maher 1999; Muxworthy et al. 2022). This magnetic PM is released as exhaust particles (Matzka and Maher 1999) and non-exhaust particles which can incorporate components from brake wear Fe, Cu, Ba, Sb, Zn, Ti and Mn (Wahlström et al. 2010; Winkler et al. 2020), tyre wear Fe, Zn, Ca, Al and Si (Panko et al. 2018; EIT Urban Mobility, 2025) and road wear Al, Ca, K, Fe, Mg and Ti (Gustafsson 2018; Alves et al. 2020). As with total urban PM, magnetic PM also occurs in various size fractions that are largely dependent on the source e.g. combustion, friction or road erosion. The distribution of urban pollution depends on factors such as the total mass of the pollutants emitted, the height of the emission, atmospheric factors, and wind conditions (Mathias et al. 2006). Due to the complex structural nature of the urban environment, it is challenging to comprehensively measure the distribution of PM pollution, let alone measuring within the urban canopy layer.

In urban environments, air quality is typically measured at fixed monitoring stations. Their high temporal accuracy is alternately limited by their low spatial representativeness, as costly equipment limits their use (Hansard et al. 2011). The spatial resolution of air quality measurements can be improved by using a method that combines environmental magnetic techniques with biomonitoring. Magnetic methods serve as a proxy for identifying ferrimagnetic minerals and related heavy metals within the PM and are useful for the identification of pollution sources, intrinsic properties, and distribution (Chaparro et al. 2020; Muxworthy et al. 2022). Magnetic biomonitoring can be applied with many different biological organisms, such as lichens, leaves and mosses, or by in situ measurements (Paoli et al. 2017; Limo et al. 2018; Castañeda-Miranda et al. 2020; Chaparro et al. 2020). Magnetic biomonitoring using moss bags provides a useful tool for monitoring airborne pollution because it is easily applied, cost-effective and allows for a variety of sampling strategies. The method provides a good spatial resolution for data collection with long sampling periods (Limo et al. 2018, 2024).

Since urban infrastructures are usually complex and cover large areas, extensive monitoring of air pollution distributions is often managed by modelling. The Gaussian line source model Contaminants in the Air from a Road - Finnish Meteorological Institute (CAR-FMI) is developed to model the dispersion of the traffic-produced pollutants at the urban scale (Härkönen 2002). CAR-FMI has been evaluated against measured PM data in several locations in Finland and the UK e.g. Kauhaniemi et al. 2008; Aarnio et al. 2016; Srimath et al. 2017. Furthermore, magnetic biomonitoring has been used in extensive magnetic PM monitoring schemes (Vuković et al. 2015; Salo and Mäkinen 2019) and street canyon studies (Hofman and Samson 2014; Lazic et al., 2016; Limo et al. 2024) to monitor urban pollution distributions. Other earlier vertical studies of PM concentrations by different techniques have used only a few specific monitoring sites (Xin et al. 2021) or a single city transect (Li et al. 2022). We have applied CAR-FMI modelling for corresponding street and roof level samples to estimate whether the accumulated magnetic PM is a representative indicator of PM dispersion calculated by the CAR-FMI model. We have studied the urban magnetic PM distribution within the urban canopy layer, which includes measurements at ground and rooftop levels. To our knowledge, this is the first study in biomonitoring research that has simultaneously conducted extensive street and roof level measurements within a larger urban area, while comparing these with urban-scale dispersion modelling (CAR-FMI) of PM and exploring the possibility of assessing the representativeness of a monitoring station.

This study aims to investigate how urban magnetic PM pollution is distributed within the urban canopy layer, the extent which the ground-level magnetic PM pollution is dispersed to the upper limits of the urban residence, and what factors might explain the differences between the concentrations. We hypothesize that magnetic PM pollution levels at higher altitudes are mostly diluted to less harmful levels. In general, we expect high magnetic PM values to correlate with high modelled PM values, but local discrepancies may occur due to varying environmental conditions and unmodelled point sources. We assume that moss bag magnetic measurements are an effective method for assessing the representativeness of air quality monitoring stations. We seek to increase knowledge and understanding of the dispersion of pollutants in the urban atmosphere. In doing so, we strive to promote healthier urban environment and responsible urban planning.

Materials and methods

Study area and sampling

The study area covers the central part of the city of Turku (ca. 9.0 km^2) in SW Finland (60°27′N, 22°16′E) (Fig. 1). Turku is the fifth largest city in Finland with a population of 197 900. According to the latest air quality survey in Turku region (FMI, 2020) the concentrations of nitrogen oxides and PM are mainly caused by traffic and long-range transport, while industry and energy production have a minor impact on the city's air quality. The contribution of exhaust emissions to $PM_{2.5}$ concentrations in Turku are low. The traffic-originated maximum annual average concentrations of $PM_{2.5}$ were ca. 2 µg/m^3 next to the busiest streets within the city centre and grid plan area. The traffic originated maximum daily $PM_{2.5}$ concentrations were 10 µg/m^3 at road intersections and 4–8 µg/m^3 on other trafficked routes (FMI, 2020). The traffic originated maximum annual average concentrations of PM_{10} were above 10 µm/m^3 next to the busiest streets and intersections within the city centre and 5–10 µg/m^3 next to other busy streets within the grid-plan area. The traffic-originated maximum daily PM_{10} concentrations were 30–50 µg/m^3 at busy streets and intersections in the city centre (FMI, 2020). Air quality is measured with two fixed monitoring stations located at the city centre Kauppatori marketplace (NO_x, $PM_{2.5}$, PM_{10}) and a nearby Ruissalo island (SO_2, NO_x, O_3) about 10 km west of the city centre (Turku, 2021). In the Turku region, air quality measuring stations are also located in neighbouring cities of Raisio (NO_x, $PM_{2.5}$ and PM_{10}), Naantali (SO_2, NO_x and PM_{10}), Kaarina (NO_x and PM_{10}) and Parainen (PM_{10}) (Turku, 2021).

Of the total number of sample sites (n=52), 48 were located within the grid plan area, and 4 were located further away from the city centre. Sampling sites were placed on both sides of the river Aurajoki, which flows east to west through the study area (Fig. 1). The study area was bounded by busy roads to the north, east and south and to the west by a harbour area in. To investigate differences in elevational behaviour of magnetic PM concentrations a total of 30 sampling sites were placed pairwise at street (St) (n=15) and

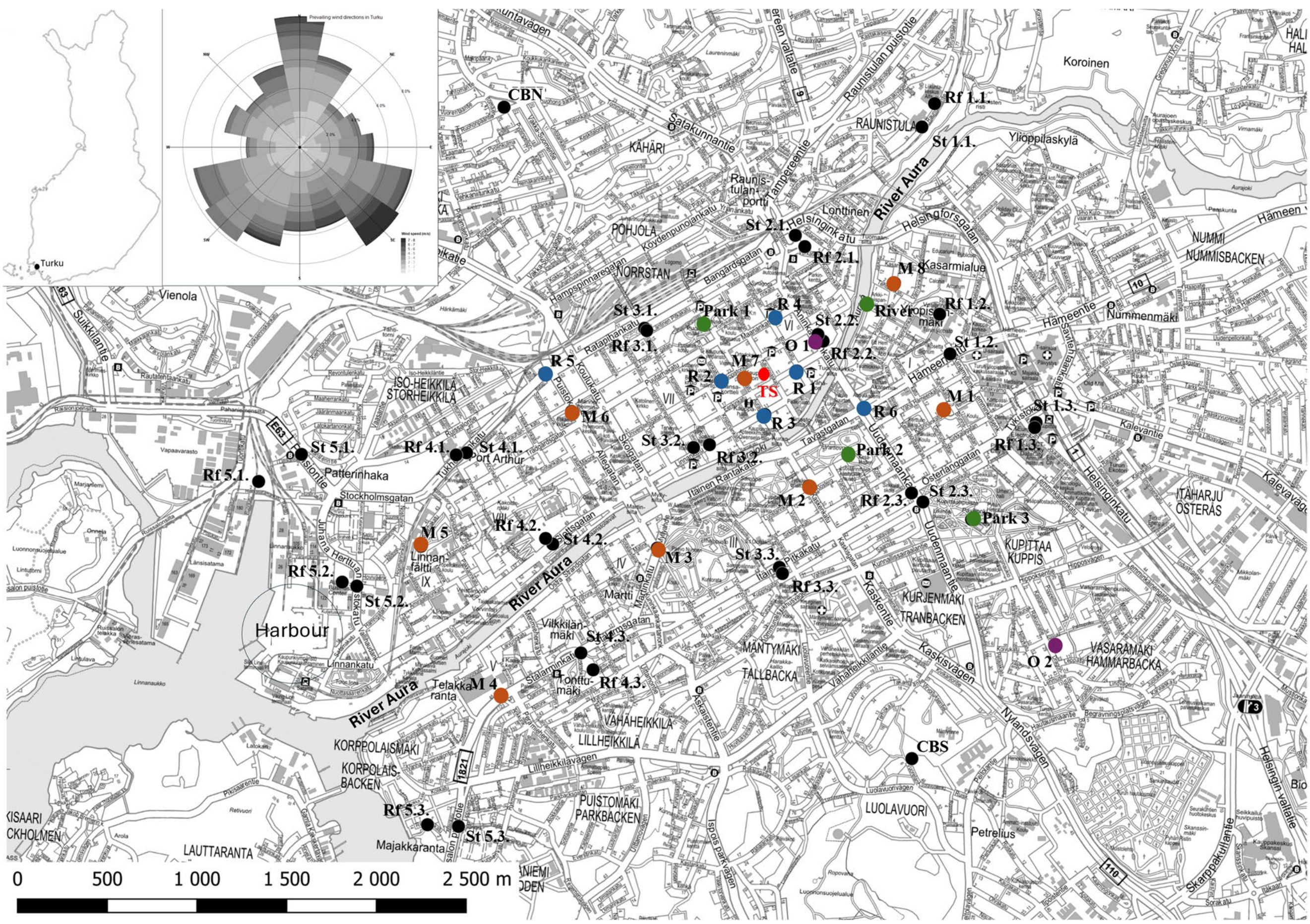

Fig. 1 Sampling locations of the street (St/black; M/brown; R/blue), roof (Rf/black), park (Park/green), river (River/green), Osiris sensor (O/purple) and Turku measuring station (TMS/red). The wind rose diagram indicates prevailing wind directions and strengths during the sampling period (FMI weather station Artukainen, Turku)

roof (Rf) ($n=15$) levels with average heights of 3.00 m and 27.30 m, respectively. Additional samples were placed on street level at the height of 3.00 m to study ground concentrations in more detail. These included 8 samples (M) approximately in the middle of each cell created by the deployment of street and roof samples and another 6 samples (R) around the city centre marketplace to assist in evaluating the representativeness of the Turku monitoring station. Furthermore, 4 sample sites were placed at parks ($n=3$) and at the riverbank ($n=1$) to reflect city background environments within the grid plan area. Additionally, four sample sites were placed at rooftops ($n=4$) further away from the grid plan area to assess city background concentrations at rooftop level. These were located 1.46 km north (CBN), 2.16 km east (CBE), 2.33 km south (CBS) and 4.52 km west (CBW) from the Kauppatori marketplace.

The sampling duration was 62 days from 28th September to 28th November in 2017. During this time the trees lost their foliage, which minimized the impact of vegetation; furthermore, icy and snowy conditions were avoided as this would influence resuspension. The average daily air temperature of the period was 4.51 °C, the prevailing wind directions from N, SE and SW, the average daily wind speed was 3.01 m s^{-1} and total rainfall was 164.26 mm. The weather conditions during the sampling period fall within the long-term averages. After the exposure period, each moss bag sample was air-dried in a Panasonic MIR-262 incubator (Panasonic Healthcare Ltd., Tokyo, Japan) at a constant 35 ℃ temperature. Dry samples were homogenized using a Retsch PM100 planetary ball mill (Retsch GmbH, Haan, Germany) using zirconium oxide (ZrO_2) jar and balls. The homogenized samples were retained in 10 cm^3 airtight plastic containers.

Sampling design

The moss bags were prepared following the Finnish standard SFS 5794 (Finnish Standards Association 1994). The *Sphagnum papillosum* moss was collected from a remote bog area near Honkajoki, Finland, far away from any road network or city/industrial areas. The moss was cleaned from unwanted vegetation and litter in the laboratory and then washed in 0.5 M HCl and rinsed with deionized H_2O to neutralize the material and balance the element levels. A part of the acid-washed moss was used for control samples (CS 1–2). Circa 15 g of damp moss was placed in a polyamide net (0.64 cm^2 mesh) and closed with a cotton thread. At each sampling site, three moss bags (subsamples) were tied to a wooden rod attached to suitable object (lamp or road signpost). To assess rural background levels, three background sites were allocated at Erikvalla ca. 14 km SE (BKGR 1), Laulainen ca. 25 km NW (BKGR 2) and Mäkkylä ca. 16 km NE (BKGR 3). The control and background magnetic and elemental values (CS 1–2 and BKGR 1–3) were subtracted from the exposed samples to present the true accumulation of pollutants during the exposure period (Table 1). Three samples (Rf 5.3, CBE and CBW) were damaged during the sampling period, and no measurements were achieved from these samples.

Magnetic measurements

Mass specific magnetic susceptibility (χ x 10^{-8} m^3 kg^{-1}) is a parameter that illustrates the concentration of magnetic minerals in a substance. Mass-specific magnetic susceptibility was measured at the Department of Geography and Geology, University of Turku, using a Bartington MS2B dual-frequency (0.47 and 4.7 kHz) susceptibility meter (Bartington Instruments Ltd., Witney, UK). Two subsamples of each sample were prepared and weighed in standard 10 cm^3 containers. The holder cup correction -0.2×10^{-5} was achieved by measuring five empty sample cups. Each subsample was measured five times with air measurements before and after sample measurement in the low frequency setting. Thus, the final value was an average of ten measurements per sample. The final mass-specific susceptibility of a sample was achieved by subtracting the average values of control moss and background samples from the initial sample χ value (Table 1).

Hysteresis loops for examining magnetic mineral composition and grain size distributions were measured at the Department of Physics and Astronomy in the University of Turku, using Quantum Design MPMS SQUID XL magnetometer (Quantum Design Inc., San Diego, USA). The measurements for the hysteresis loops were done at 300 K in an oscillating magnetic field up to positive and negative 1 T. Between 1 T – 1 mT magnetization was measured in intervals of 0.3 mT and between 1 mT and −1 mT in intervals of 0.1 mT. Saturation magnetization (M_S), saturation remanence (M_{RS}) and coercive force (H_C) were obtained by subtracting the linear diamagnetic signal from the 1 ml sample cup, sample holder and K of moss using a fitting function:

$$M\left(B\right) = M_S \times ArcTan\left(\frac{B \pm B_C}{c}\right)$$

to both ascending and descending hysteresis loop branches. Here M(B) is the magnetization induced by a magnetic field (B). M_S is the saturation magnetization, B_C the coercive force and c is used as a scaling constant. Instead of measuring the coercivity of remanence (B_{CR}) from the backfield, the value was attained by numerically finding the field at the maximum of the derivative of ΔM curve (Jackson et al. 1990).

Table 1 Summary of statistics for mass-specific magnetic susceptibility (χ x $10^{-8}m^3kg^{-1}$) and element concentrations (mg kg^{-1}) at different sampling locations

	χ	Al	Ba	Cu	Fe	Mn	Ti	V	Zn	Na	Ca	Mg
Street samples												
Min	5.30	250.00	2.20	5.59	430.00	3.00	21.00	1.00	6.30	110.00	500.00	150.00
Max	66.15	750.00	21.70	45.86	2210.00	27.00	84.00	5.00	149.20	1460.00	2200.00	510.00
Mean	15.15	430.00	8.78	12.89	944.67	13.87	46.40	2.87	46.77	472.00	1073.33	299.33
Median	10.95	450.00	9.50	9.89	880.00	14.00	43.00	3.00	26.80	390.00	1100.00	270.00
stdv	14.88	156.75	4.73	9.90	442.85	6.88	17.90	1.13	43.02	347.11	435.02	114.42
Roof samples												
Min	0.90	50.00	3.20	2.36	110.00	0.00	4.00	0.00	5.90	420.00	500.00	150.00
Max	13.00	250.00	14.60	13.87	550.00	81.00	18.00	3.00	113.40	1050.00	2300.00	480.00
Mean	5.76	164.29	7.11	5.87	313.57	24.79	11.21	1.50	35.72	691.43	1014.29	317.14
Median	4.88	150.00	6.80	4.81	275.00	21.00	10.50	1.50	25.90	680.00	950.00	290.00
stdv	3.26	53.45	2.69	3.24	120.74	19.43	4.14	0.76	30.34	178.10	468.81	107.45
park and river samples												
Min	1.65	50.00	0.00	0.88	90.00	0.00	3.00	0.00	0.00	90.00	100.00	10.00
Max	3.50	150.00	2.40	3.25	200.00	12.00	8.00	1.00	228.50	340.00	400.00	110.00
Mean	2.98	75.00	1.55	2.17	145.00	4.75	6.00	0.25	63.20	197.50	275.00	75.00
Median	3.38	50.00	1.90	2.28	145.00	3.50	6.50	0.00	12.15	180.00	300.00	90.00
stdv	0.89	50.00	1.06	1.21	63.51	5.12	2.45	0.50	110.79	122.85	125.83	45.09
All street samples (St, M, R)												
Min	1.45	50.00	0.20	1.73	90.00	0.00	5.00	0.00	0.70	20.00	300.00	50.00
Max	66.15	750.00	70.00	45.86	2210.00	27.00	84.00	5.00	405.80	1460.00	2200.00	510.00
Mean	12.79	346.43	8.96	10.99	753.57	11.18	36.25	2.29	48.05	366.79	889.29	237.50
Median	10.43	350.00	6.00	9.35	705.00	11.00	34.00	2.00	20.85	280.00	800.00	240.00
stdv	12.31	179.47	12.80	8.49	457.52	7.01	20.92	1.36	78.43	309.80	433.20	128.02
Control and background samples												
ctrl 1	−1.36	0.01	1.6	1.06	0.02	0.4	3	1	1.4	0.005	0.01	0.002
ctrl 2	−1.20	0.01	1.7	1.12	0.03	0.5	3	1	1.9	0.005	0.01	0.003
bkgr 1	−0.20	0.005	2.9	1.51	0.02	20.0	4	1	9.6	0.03	0.02	0.012
bkgr 2	−0.35	0.005	5.3	1.41	0.02	4.0	4	1	22.9	0.014	0.01	0.008
bkgr 3	−0.10	0.005	5.0	1.37	0.02	3.0	4	1	24.1	0.013	0.01	0.008

The values account for control and background data

Monitoring sensors

The representativeness of the official monitoring station at Turku city centre was examined by two separate sensors illustrating concentrations of airborne particulates at additional locations within the study area. The local PM_{10} concentrations were measured using Osiris airborne particulate monitor (Turnkey Instruments Ltd., Cheshire, UK). The other sensor was placed next to a busy street Aninkaistenkatu (circa 22 500 veh/day) in the city centre and the other to a small housing residential district Vasaramäki circa 2.2 km SE from the city centre (Fig. 1). At Aninkaistenkatu (O1) the sensor was located on the roof of a small business building at a height of 4 m and 8 m away from the street curb and at Vasaramäki (O2) on the roof of a small housing building at a height of 6 m (Fig. 2). The continuous measuring period of PM_{10} concentrations with Osiris sensors took place between 2nd of October and 26th of November. Moss bag samples were attached to the frames of the sensors to measure the accumulation on magnetic PM during the measuring period of the sensors.

CAR-FMI dispersion modelling

Study area and period

The local scale dispersion model CAR-FMI was used for the dispersion computations to produce the road increment concentrations of $PM_{2.5}$ and PM_{10}. Computations for Turku region were made for the whole study period and calculated to identical locations with the moss biomonitoring sites ($n = 52$) and air quality monitoring sites ($n = 3$). The computation heights vary from 3 m to 47 m.

Dispersion model

The local scale dispersion model CAR-FMI (Contaminants in the Air from a Road – Finnish Meteorological Institute, e.g. Härkönen 2002) is a mathematical model for predicting

Fig. 2 Osiris monitoring sensors and moss bag sample collectors at Aninkaistenkatu (above) and at Vasaramäki (below)

the dispersion of traffic-related pollution from an open road network. The model computes the concentrations of carbon, nitrogen monoxides, nitrogen dioxide, nitrogen oxides, ozone, and particulate matter. The model builds upon a partly analytical solution of the Gaussian diffusion equation for a finite line source. The dispersion parameters are modelled as function of the Monin–Obukhov length, the friction velocity, and the mixing height. The model includes a treatment for the basic reactions of nitrogen oxides, oxygen and ozone, using a receptor-oriented discrete parcel method, and the dry deposition of the particles. The properties of input data (traffic, emissions, and meteorological variables) are assumed to be constant during each hour.

Traffic volume

The link-based annual average daily traffic flow (AADT) of the Turku region air quality survey (FMI, 2020) in 2018 was scaled to 2017 with the ratio of mileage in 2017 and 2018 in LIPASTO (Eckhardt 2019a, b). LIPASTO is a calculation system for traffic exhaust emissions and energy consumption in Finland. The system comprises two separate units, the emission inventory part and the unit emission database part (Mäkelä and Auvinen 2009). The road links in the AADT data are classified as either public roads, or as roads belonging to a specific municipality (Turku). The LIPASTO mileage values for the corresponding municipality were applied in scaling the data for municipality roads. For public roads, the sum of mileage values for the five municipalities in the area was used for scaling. Hourly, day-of-week, and monthly variation of traffic volume are the same as in FMI (2020) survey.

The share of heavy traffic for each road link was based on AADT data. The share of buses and trucks within heavy traffic, as well as the share of cars and vans, is based on LIPASTO mileage data of Turku in 2017 (Eckhardt 2019a). Mileage data for streets were applied for road links with speed limit $<$ 60 km/h, and data for roads for road links with speed limit $\geq$ 60 km/h.

Exhaust PM emission data

We have used PM exhaust emission factors calculated from the PM emission and mileage data in Turku 2017 of LIPASTO (Eckhardt 2019a). The emission factors are estimated separately for public roads (= average value) for four vehicle types (cars, vans, buses and trucks), and for streets and roads (Table S1). The street and road type of emission factor was used for roads with speed limit $<$ 60 km/h and $>$ 60 km/h, respectively.

Non-exhaust PM emission data

The road dust emission model FORE (Forecasting Of Road dust Emissions; Kauhaniemi et al. 2011; Omstedt et al. 2005) was used. The computation of non-exhaust emission factors requires information of the reference emission factors, hourly meteorological data, roughness length, share of studded tyres, as well as date and time of the street sanding. The reference emission factors of 30–150 mg/veh/km ($PM_{2.5}$) and 200–1200 mg/veh/km (PM_{10}) are based on Omstedt et al. (2005). The roughness length represents the roughness of road surroundings, such as buildings and trees. For Turku, a roughness length value of 0.5 m was used. The transition from summer to winter tyres utilizes the weekly counting of vehicles with studded tyres in Helsinki (REDUST, 2014). The maximum annual share of vehicles using studded tyres is 80% (Lahti and Sainio 2021; Kupiainen 2007). Thus, the assumed share of studded tyres increases from 0% to 73.8% during the study period. The sanding dates were modelled by FORE based on meteorological conditions. Thus, there were 10 sanding days during the study period. As no information of the sanding hours were available, sanding was assumed to occur at 6 a.m.

Meteorological data

Meteorological data for dispersion modelling were based on observational data and meteorological pre-processing model MPP-FMI (Meteorological Pre-Processing - the Finnish Meteorological Institute; Karppinen et al. 2000). The primary hourly weather observation data were obtained from the Turku Artukainen station, located approximately 5 km west of the market square at the city centre. In addition, wind speed and direction data were provided by the weather station of Turku Rajakari, located approximately 12 km southwest of the city centre. The hourly weather data were downloaded from FMI data base.

The estimation of boundary layer height was based on hourly weather and sounding data, including vertical temperature and pressure profiles for noon and midnight from the Jokioinen observatory, located 80 km northeast of Turku. The sounding data were downloaded from FMI data base.

Background data

The hourly background concentrations of $PM_{2.5}$ and PM_{10} concentrations of Raisio Ihala monitoring station were added to road increment to obtain the total concentrations. Raisio Ihala monitoring station with 3 m monitoring height is situated at residential area of detached houses. About 300 m to the east of the station, there is a busy street (Turku 2017). The measurement data of the Raisio Ihala station was available from 17th of August 2017. These data were downloaded from FMI open data (FMI, 2024). Single missing observations were replaced by interpolation and longer gaps by using data from the previous corresponding hour.

Chemical analyses

Element concentrations (mg kg^{-1}) of moss bag samples were analysed for Al, Ba, Cu, Fe, Mn, Ti, V, Zn, Ca, Mg and Na in the accredited laboratory AcmeLabs, Canada. The VG101 analysis method uses 1 g sample split, digested first in HNO_2 then in Aqua Regia and then analysed by inductively coupled plasma mass spectrometry (ICP-MS). To ensure the acceptability of the results, the laboratory method standard includes ratification measurements using two procedural blanks, two reference materials (STD CDV-1 and STD V16), and two QC protocol sample duplicates. Element concentrations of control moss and background sample averages were subtracted from the initial moss bag raw data (Table 1).

Statistical data analyses

The statistical analyses were calculated with IBM SPSS Statistics version 27. The normality of the mass-specific magnetic susceptibility (χ) and element concentration data was tested with the Shapiro-Wilk test. Not all tested variables followed normal distributions, and therefore, Spearman's rank order correlation coefficient was used to determine the statistical significance of the correlation between magnetic and element parameters. Linear regression was used to determine the relationship between magnetic susceptibility χ and CAR-FMI modelled PM_{10} concentrations. The statistical significance of differences between street and roof values were tested by using the non-parametric Mann-Whitney U test. Multivariate analyses, principal component analysis (PCA) and cluster analysis (CA) were used to identify sources of the elements. Before computing the data for PCA and CA, standardization was performed to remove any issues scaling within the variables. PCA with VARIMAX normalized rotation was applied to extract principal factors from the elemental component variables. For this study the Kaiser-Meyer-Olkin (KMO) value (KMO > 0.60) and significant result of Bartlett's test of sphericity ($p < 0.05$) were accepted. Principal factors with eigenvalues > 1.0 were retained with the support of scree plots. Total cumulative variance of the selected factors is to explain over 80% of total variance, and factor loadings higher than 0.7 were regarded as suitable. CA with the application of Euclidean distances for variables as a measure of distance and Ward's method as a linkage rule were performed for forming clusters from element concentration data.

Results

Magnetic susceptibility

Mass specific susceptibilities (χ) varied between 5.30×10^{-8} m^3 kg^{-1} and 66.15×10^{-8} m^3 kg^{-1} within the street samples (St), and between 0.90×10^{-8} m^3 kg^{-1} and 13.00×10^{-8} m^3 kg^{-1} within the roof samples (Rf) (Table 1). The maximum roof (Rf) values correspond to mean (12.79×10^{-8} m^3 kg^{-1}) of all street samples (St, M and R). The highest mass-specific magnetic susceptibility values at street level were found on sample sites (St) 2.1., 2.2., 2.3., 4.3., (5.1) and (5.2) (Table 2), and at roof level on sample sites (Rf) 2.1., 2.2., 2.3. and 3.1. (Table 3). At street sample sites (St) 2.1., 2.2. and 2.3. traffic volumes vary between circa 16 000–22 500 vehicles per day, at sample site (St) 4.3. traffic volumes are just above 17 000 vehicles per day, and at sample sites (St) (5.1) and (5.2) about 6 000 and 13 000 vehicles per day, respectively, but they are subject to peak volumes due to on- and off-traffic from ferries from the nearby harbour. The roof sample sites (Rf) 2.1., 2.2. and 2.3. are located at the same street section as the corresponding street samples. The roof sample site (Rf) 3.1. is in the vicinity of the train station and a street section with traffic volumes approximately 6 000 vehicles per day; however, 65 m north is a busy street with traffic volumes around 28 000 vehicles per day.

Table 2 Summary of statistics for sample height, annual average daily traffic flow (AADT), CAR-FMI average concentrations for $PM_{2.5}$ and PM_{10} (µg/m^3), CAR-FMI sum concentrations for $PM_{2.5}$ and PM_{10} (µg/m^3), mass-specific magnetic susceptibility (χ x 10^{-8}m^{3}kg^{-1}) and element concentrations (mg kg^{-1}) at street (St) level sample sites

	Street 1.1.	Street 1.2.	Street 1.3.	Street 2.1.	Street 2.2.	Street 2.3.	Street 3.1.	Street 3.2.
Height (m)	3.00	3.00	3.00	3.00	3.00	3.00	3.00	3.00
AADT	1494	**17,373**	5879	**15,944**	**22,520**	**16,033**	6178	1993
$PM_{2.5}$ avg.	4.65	**5.48**	**5.26**	**6.02**	**5.74**	**5.22**	**5.43**	5.11
PM_{10} avg.	8.59	**10.79**	**10.13**	**11.89**	**11.34**	**10.01**	**10.36**	9.61
$PM_{2.5}$ sum	6920.23	**8154.22**	**7833.28**	**8961.19**	**8544.83**	**7764.14**	**8080.62**	7599.82
PM_{10} sum	12785.68	**16061.29**	**15066.52**	**17692.30**	**16869.36**	**14898.68**	**15417.72**	14304.67
X	5.30	7.75	10.95	**15.80**	**66.15**	**22.65**	5.95	8.05
Al	250.00	250.00	**550.00**	350.00	**750.00**	**450.00**	250.00	250.00
Ba	4.00	8.00	**9.80**	**12.20**	**21.70**	**10.30**	2.20	**10.60**
Cu	5.59	6.53	9.89	**13.63**	**45.86**	**18.92**	7.07	8.74
Fe	600.00	430.00	**1000.00**	890.00	**2210.00**	**1150.00**	550.00	520.00
Mn	9.00	3.00	**15.00**	12.00	**27.00**	**16.00**	3.00	12.00
Ti	30	21	**65**	42	**84**	**48**	28	24
V	2	1	**4**	**4**	**5**	**3**	1	**3**
Zn	13.2	6.3	34.8	**79.1**	**52.1**	**17**	7.8	26.8
Na	460	220	**480**	470	**820**	390	110	270
Ca	600	500	1500	**1200**	**2200**	1000	500	800
Mg	260	150	**430**	270	**510**	**310**	160	160

	Street 3.3.	Street 4.1.	Street 4.2.	Street 4.3.	Street 5.1.	Street 5.2.	Street 5.3.	Average
Height (m)	3.00	3.00	3.00	3.00	3.00	3.00	3.00	3.00
AADT	**12,481**	**11,958**	8569	**17,313**	**13,316**	6078	**18,035**	11,678
$PM_{2.5}$ avg.	**5.24**	5.12	4.93	**5.27**	4.83	4.75	4.85	5.19
PM_{10} avg.	**9.98**	9.78	9.31	**10.14**	9.19	8.91	9.12	9.94
$PM_{2.5}$ sum	**7798.35**	7624.74	7340.31	**7837.29**	7180.44	7074.70	7210.61	7728.32
PM_{10} sum	**14857.63**	14549.30	13847.62	**15090.42**	13676.26	13257.32	13572.48	14796.48
X	10.00	11.45	7.95	**15.65**	**15.85**	**15.25**	8.55	15.15
Al	350.00	**450.00**	350.00	**550.00**	**650.00**	**550.00**	**450.00**	430.00
Ba	**10.30**	6.20	4.40	7.70	**11.10**	**9.50**	3.70	8.78
Cu	9.06	10.59	6.48	**13.99**	**14.27**	**14.90**	7.82	12.89
Fe	760.00	880.00	700.00	**1120.00**	**1250.00**	**1310.00**	800.00	944.67
Mn	**14.00**	**15.00**	**15.00**	**14.00**	**23.00**	**23.00**	7.00	13.87
Ti	40	43	40	**58**	**68**	**62**	43	46.40
V	2	**3**	**3**	**3**	**4**	**3**	2	2.87
Zn	**149.2**	**104.5**	12.3	19.1	**72.9**	**89.1**	17.3	46.77
Na	220	**640**	210	360	**1460**	**780**	190	472.00
Ca	**1100**	**1200**	**1100**	1000	**1400**	**1200**	800	1073.33
Mg	260	290	260	**310**	**490**	**410**	220	299.33

The bolded values indicate concentrations above the average street concentration of each element on individual row

Within the additional samples (M and R) the mass-specific magnetic susceptibilities varied between 1.45×10^{-8} m^3 kg^{-1} and 27.05×10^{-8} m^3 kg^{-1}, and within park and river samples between 1.65×10^{-8} m^3 kg^{-1} and 3.50×10^{-8} m^3 kg^{-1} (Tables 1 and 4). In addition to street sample sites (St) 2.1., 2.2., 2.3., 4.3., (5.1) and (5.2) mentioned above, the highest mass-specific magnetic susceptibility values were also found on sample sites M3, R4, R5 and R6. At sample sites R5 and R6, the traffic volumes are circa 20 000 and 15 500 vehicles per day, respectively. At sample site M3, traffic volumes are circa 17 000 vehicles per day, and at sample site R4 circa 10 000 vehicles per day. Relatively high mass-specific magnetic susceptibility values (χ) were found on street sample sites (St) 1.3. (10.95), 3.3. (10.00) and 4.1. (11.45) as well as on R1 (11.10) and R3 (10.85). At sites (St) 1.3., 3.3. and R3 traffic volumes are approximately 6 000, 12 500 and 7 000 vehicles per day, and at sites (St) 4.1. and R1 about 12 000 and 5 500 vehicles per day, respectively.

Park sample sites 2 (1.65) and 3 (3.50) were close to roads with traffic volumes ca. 11 000 and 2500 vehicles per day (Table S2); however, the sample moss bags were placed well within the park area and a notable distance away from the busy roads, 250 m and 200 m, respectively. Sample sites Park 1 (3.50) and River (3.25) were not in the vicinity of any

Table 3 Summary of statistics for sample height, CAR-FMI average concentrations for $PM_{2.5}$ and PM_{10} (µg/m^3), CAR-FMI sum concentrations for $PM_{2.5}$ and PM_{10} (µg/m^3), mass-specific magnetic susceptibility (χ x $10^{-8}m^3kg^{-1}$) and element concentrations (mg kg^{-1}) at roof (Rf) level sample sites

	Rf 1.1.	Rf 1.2.	Rf 1.3.	Rf 2.1.	Rf 2.2.	Rf 2.3.	Rf 3.1.	Rf 3.2.
Height (m)	16.00	16.00	33.50	26.50	25.00	24.00	26.50	29.00
$PM_{2.5}$ avg.	4.62	**4.83**	4.70	**4.88**	**4.79**	**4.74**	**4.83**	**4.77**
PM_{10} avg.	8.57	**9.06**	**8.83**	**9.20**	**8.96**	**8.87**	**9.08**	**8.93**
$PM_{2.5}$ sum	6878.09	**7188.49**	6993.38	**7255.14**	**7120.98**	**7050.09**	**7190.64**	**7103.26**
PM_{10} sum	12745.75	**13487.63**	**13144.33**	**13683.61**	**13337.12**	**13197.39**	**13505.35**	**13285.13**
X	3.60	3.80	4.35	**9.80**	**13.00**	**8.65**	**9.00**	5.05
Al	150.00	150.00	150.00	150.00	**250.00**	150.00	**250.00**	150.00
Ba	6.70	3.20	6.80	7.00	**8.60**	6.20	7.00	6.80
Cu	3.93	3.83	3.79	**9.12**	**13.87**	**8.83**	**8.96**	5.60
Fe	240.00	230.00	280.00	**450.00**	**550.00**	**380.00**	**470.00**	270.00
Mn	29.00	10.00	10.00	19.00	22.00	19.00	23.00	20.00
Ti	8	9	**12**	**13**	**17**	**14**	**18**	9
V	0	**2**	1	**2**	**2**	**2**	**2**	1
Zn	30.5	19.4	14	22.7	34.9	33.3	22.7	17.4
Na	530	420	530	670	**780**	**810**	**740**	670
Ca	1000	600	800	800	1000	900	**1100**	900
Mg	480	190	230	280	**350**	270	**330**	260

	Rf 3.3.	Rf 4.1.	Rf 4.2.	Rf 4.3.	Rf 5.1.	Rf 5.2.	Rf 5.3.	Average
Height (m)	24.50	18.50	43.00	28.50	47.00	24.00	(55.00)	27.30
$PM_{2.5}$ avg.	**4.76**	**4.72**	4.60	4.65	4.48	4.54	n/a	4.71
PM_{10} avg.	**8.90**	**8.83**	8.57	8.67	8.31	8.43	n/a	8.80
$PM_{2.5}$ sum	**7083.01**	**7028.37**	6846.67	6916.99	6667.68	6761.97	n/a	7006.05
PM_{10} sum	**13247.13**	**13142.18**	12750.66	12902.92	12359.57	12541.59	n/a	13095.03
X	4.00	4.70	**5.90**	2.35	0.90	5.60	n/a	5.76
Al	150.00	150.00	150.00	50.00	150.00	**250.00**	n/a	164.29
Ba	3.60	6.8	**7.60**	5.10	**8.60**	**14.60**	n/a	7.04
Cu	3.57	4.64	4.98	2.55	2.36	6.12	n/a	5.87
Fe	220.00	250.00	**350.00**	110.00	210.00	**380.00**	n/a	313.57
Mn	0.00	**26.00**	**28.00**	14.00	**81.00**	**46.00**	n/a	24.79
Ti	9	9	**14**	4	6	**15**	n/a	11.21
V	1	**2**	1	1	1	**3**	n/a	1.50
Zn	5.9	**43.5**	29.1	20.5	**92.8**	**113.4**	n/a	35.72
Na	640	690	**810**	**910**	430	**1050**	n/a	691.43
Ca	500	**1200**	**2300**	500	1000	**1600**	n/a	1014.29
Mg	150	300	**420**	240	**480**	**460**	n/a	317.14

The bolded values indicate concentrations above the average roof concentration of each element on individual row

busy roads. The city background roof sample site in south (CBS) shows lower χ (1.45) and element concentrations than at north (CBN) (6.25). Circa 150 m south of sample site CBS goes a road with traffic volumes circa 4 000 vehicles per day, whereas about 850 m southeast from sample site CBN goes the Naantali highway, where traffic volumes vary between 35 000–42 000 vehicles per day.

Magnetic mineralogy

Hysteresis loops are characterised with thin loop curves and rapid saturations at 0.2–0.3 T (Fig. 3). M_S and M_{RS} range between 2.56 and 10.47 (mAm^2 kg^{-1}) and 0.04–1.49 (mAm^2 kg^{-1}) for street samples, and between 1.6 and 4.78 (mAm^2 kg^{-1}) and 0.15–0.27 (mAm^2 kg^{-1}) for roof samples, respectively. H_C and B_{CR} values range between 2.95 and 10.47 mT and 28.17–45.81 mT (Derivative DeltaM) for street samples, and 1.69–4.78 mT and 31.25–43.73 mT (derivative DeltaM) for roof samples, respectively (Table S3). Our mean B_{CR} values are 35.94, 36.86 and 36.99 mT for street (St), roof (Rf) and all street (St, M, R) samples, respectively. The hysteresis curves have a slightly slanted shape, which might imply presence of superparamagnetic (SP) particles, which give no hysteresis. The grain sizes of the magnetic particles were investigated by applying the ratios of hysteresis parameters M_{RS}/M_S and B_{CR}/B_C into the Day plot (Fig. 4). The distribution of the hysteresis ratios in the Day plot stretches from the pseudo-single-domain (PSD) region

Table 4 Summary of statistics for sample height, annual average daily traffic flow (AADT), CAR-FMI average concentrations for $PM_{2.5}$ and PM_{10} (µg/m^3), CAR-FMI sum concentrations for $PM_{2.5}$ and PM_{10} (µg/m^3), mass-specific magnetic susceptibility (χ x $10^{-8}m^3kg^{-1}$) and element concentrations (mg kg^{-1}) at additional (M and R) street sample sites.

	M 1	M 2	M 3	M 4	M 5	M6	M 7	M 8
Height (m)	3.00	3.00	3.00	3.00	3.00	3.00	3.00	3.00
AADT	1993	9167	**17,139**	**17,313**	1993	**18,136**	1993	1993
$PM_{2.5}$ average	4.95	5.06	**5.65**	5.14	4.72	**5.40**	5.11	4.91
PM_{10} average	9.23	9.54	**11.11**	9.99	8.77	**10.40**	9.48	9.15
$PM_{2.5}$ sum	7363.77	7536.07	**8413.03**	7652.90	7016.52	**8031.61**	7598.11	7299.26
PM_{10} sum	13736.05	14189.88	**16532.55**	14861.55	13044.44	**15481.41**	14110.71	13621.52
Χ	1.45	n/a	**27.05**	8.05	5.35	5.30	4.05	2.65
Al	50.00	n/a	**650.00**	250.00	350.00	**150.00**	150.00	150.00
Ba	0.70	n/a	**70.00**	4.30	3.00	1.40	3.70	3.80
Cu	1.73	n/a	**18.79**	6.60	3.83	4.53	5.10	1.90
Fe	90.00	n/a	**1490.00**	520.00	550.00	290.00	260.00	190.00
Mn	6.00	n/a	**22.00**	11.00	6.00	0.00	2.00	8.00
Ti	5	n/a	**73**	29	35	12	11	11
V	0	n/a	**4**	2	2	1	1	0
Zn	**405.8**	n/a	34.3	17.7	6.3	2.5	5.3	42.1
Na	60	n/a	350	200	290	220	110	60
Ca	300	n/a	**1200**	700	700	400	500	400
Mg	60	n/a	**390**	180	**240**	80	100	110
	R1	R2	R3	R4	R5	R6	average	
Height (m)	3.00	3.00	3.00	3.00	3.00	3.00	3.00	
AADT	4683	1494	6975	**10,263**	**19,830**	**15,645**	9186	
$PM_{2.5}$ average	**5.30**	4.97	**5.30**	**5.44**	**5.90**	**5.76**	5.22	
PM_{10} average	**10.03**	9.23	**10.09**	**10.44**	**11.87**	**11.23**	9.99	
$PM_{2.5}$ sum	**7879.04**	7401.41	**7887.55**	**8089.33**	**8781.68**	**8570.98**	7774.00	
PM_{10} sum	**14926.21**	13741.55	**15009.58**	**15538.50**	**17655.41**	**16713.90**	14865.88	
Χ	11.10	2.98	10.85	**25.45**	**13.65**	**12.95**	12.79	
Al	150.00	150.00	150.00	**350.00**	**350.00**	**350.00**	346.43	
Ba	3.90	0.20	3.40	**10.20**	5.80	8.80	8.96	
Cu	10.46	5.25	9.63	**21.06**	**11.78**	**13.77**	10.99	
Fe	480.00	190.00	490.00	**950.00**	710.00	720.00	753.57	
Mn	5.00	0	7.00	**16.00**	11.00	9.00	11.11	
Ti	18	8	18	**38**	33	28	36.25	
V	1	0	2	**4**	2	2	2.29	
Zn	18.8	22.6	0.7	46.7	13.3	27.7	48.05	
Na	340	20	30	**740**	**550**	220	366.79	
Ca	700	300	600	**1400**	**900**	700	889.29	
Mg	120	50	90	**330**	**240**	170	237.50	

The bolded values indicate concentrations above the average (St, M, R) concentration of each element on individual row

Samples sites (M) are located in the middle of the cell created by the street and roof samples and samples sites (R) are located around the Turku marketplace to assist in evaluating representativeness of Turku monitoring station

(1–15 µm) (Dunlop 2021) towards the multidomain (MD) region but settling closer to the boundary of small multidomain (MD) grains (Dunlop 2002). The hysteresis ratios fall well beneath the superparamagnetic-single domain (SP+SD) theoretical mixing curve but ultimately settle somewhat between the SP-PSD and SD-MD mixing curves (Dunlop 2002). Data settling within this area may cause difficulties in interpretation (Dunlop 2002). The domain states plot above the MD region but there seems to be a slight shift towards PSD region in the assembly of the roof level distribution ratios with respect to street level ratios.

Element concentrations

Chemical analysis for moss bags ($n=61$) included two control and three background samples. The element abundance orders for street and roof samples are as follows: Ca>Fe>Na>Al>Mg>Zn>Ti>Mn>Cu>Ba>V and Ca>Na>Mg>Fe>Al>Zn>Mn>Ti>Ba>Cu>V, respectively (Table 1).

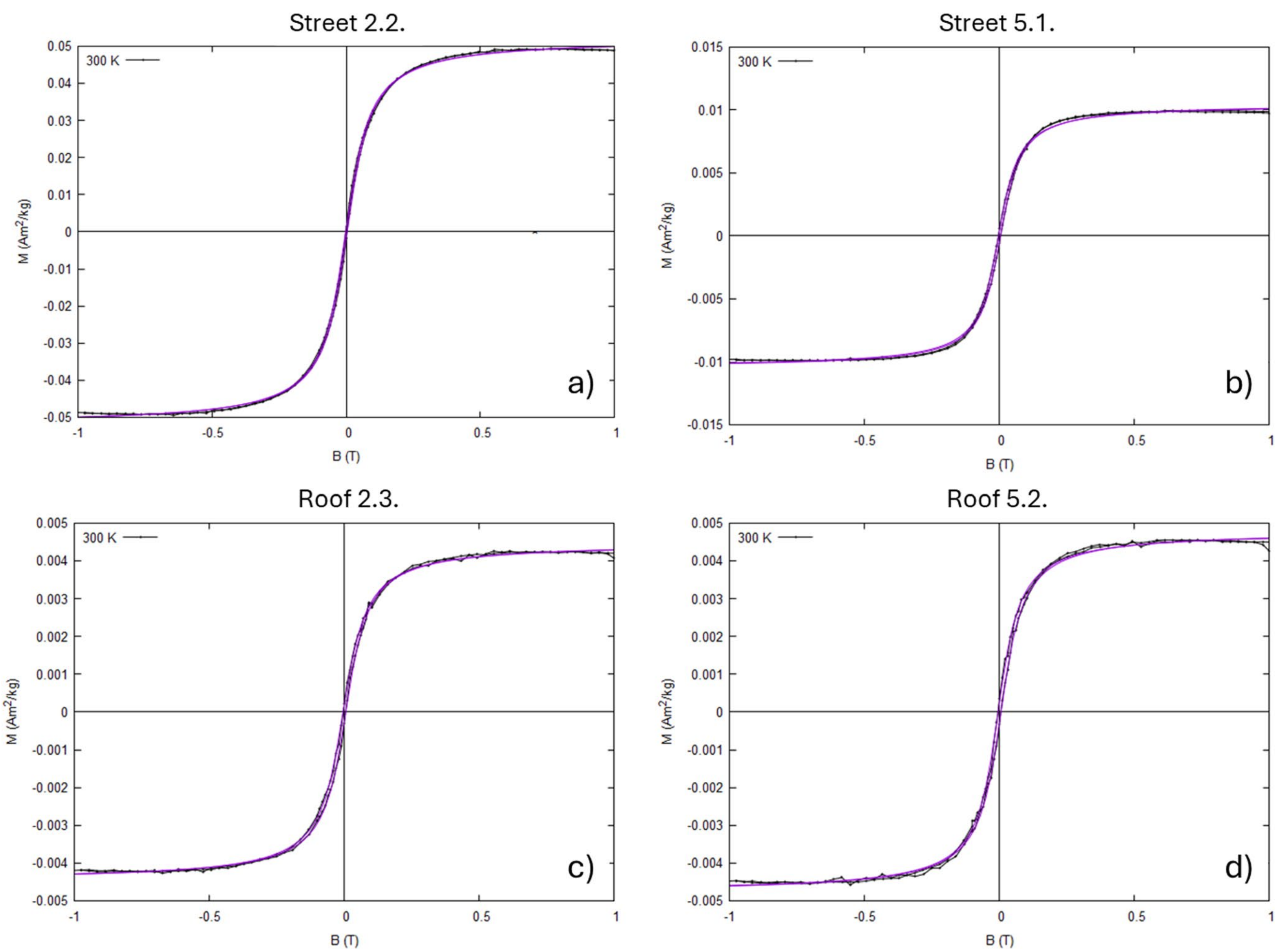

Fig. 3 Hysteresis loops of chosen sample sites (**a**) Street 2.2. (**b**) Street (5.1) **c**) Roof 2.3. **d**) Roof (5.2) measured at 300 K. Magnetic field B (T) illustrated on the x-axis and magnetization M (Am^2/kg) on y-axis

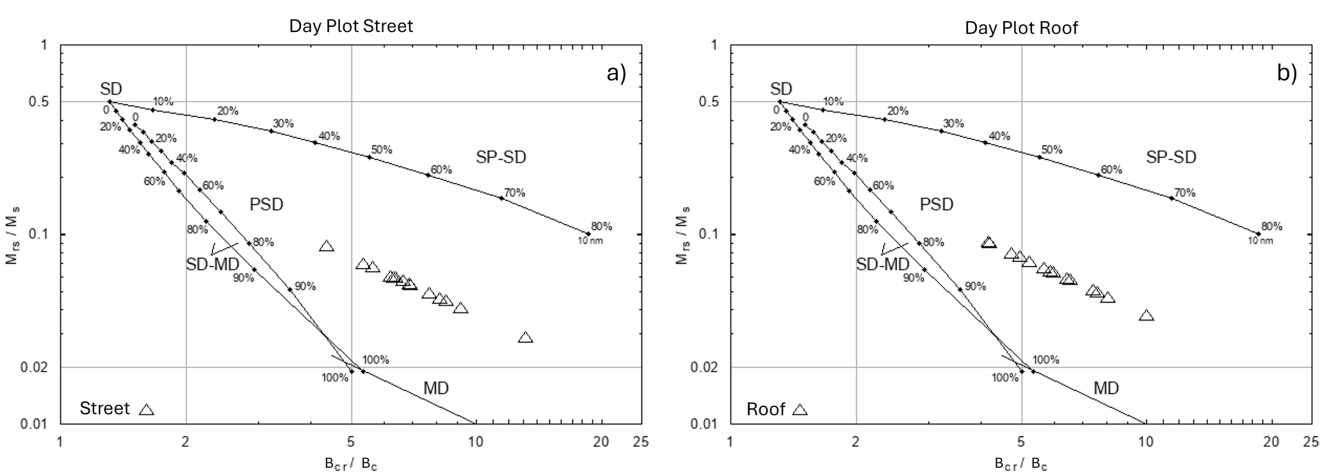

Fig. 4 Day plot of the ratios M_{RS}/M_S and B_{RC}/B_C for all (**a**) Street (St) (*n* = 15) (**b**) Roof (Rf) (*n* = 15) moss bag samples measured at 300 K. Single-domain (SD), superparamagnetic (SP), pseudo-single-domain (PSD) and multidomain (MD) boundaries for grains and mixing lines are shown after Dunlop (2002). B_{RC}/B_C ratios illustrated on the x-axis and M_{RS}/M_S ratios on y-axis

Within all street samples (St, M and R), the element abundance order is identical to street samples (St) listed above. The abundance orders are different between street and roof samples, as at roof level Ca, Na and Mg have the highest concentrations over Fe; moreover, Mn and Ti, and Ba and Cu have interchanged their positions. The highest concentrations for the elements (Al, Ba, Cu, Fe, Mn, Ti, V, Zn, Na, Ca and Mg) are found on street sample sites (St) 1.3., 2.1., 2.2., 2.3., 4.3., (5.1) and (5.2) (Table 2). At street sample sites (St) 3.3. and 4.1., high concentrations are found, but with fewer elements (Al, Ba, Mn, Zn, Na and Ca). The highest element concentrations in the roof samples are found on sample sites (Rf) 2.1., 2.2. 2.3., 3.1., 4.2., (5.1) and (5.2) (Table 3). Within the additional sample sites, the highest element concentrations are found on sample sites M3, R4 and R5 (Table 4).

CAR-FMI modelling

The CAR-FMI modelling results are presented for each corresponding moss bag sample location (Tables 2, 3 and 4). The intercomparison of the values of modelled average and sum concentrations for $PM_{2.5}$ and PM_{10} and magnetic PM concentrations shows consistency with street samples (St) 2.1.,2.2., 2.3. and 4.3. where all the values are higher than their corresponding averages, and with samples 1.1., 3.2., 4.2. and 5.3. where all the values are lower than their corresponding averages (Table 2). A moderate consistency is shown with street samples (St) 1.3., 3.3. and 4.1. where the value of χ is high but lower than the average value, and the modelled concentration is higher than the average value (Tabel 2). The CAR-FMI model gives a higher value of modelled concentration against a low value of χ for street samples (St) 1.2. and 3.1., and a lower value of modelled concentration against a high value of χ for street samples (St) (5.1) and (5.2) The CAR-FMI model and magnetic PM concentrations show consistency with roof samples (Rf) 2.1., 2.2., 2.3. and 3.1., both being higher than the averages, and with 1.1., 4.3., 5.1. and 5.2., both being lower than the averages. For roof samples (Rf) 1.2., 1.3., 3.2., 3.3. and 4.1. the model results are higher (Table 3). Within the additional sampling sites, the model shows consistency with measurements M3, R4, R5 and R6, both values being higher than their corresponding averages and with M1, M4, M5, M7, M8 and R2, both values being lower than their corresponding averages. The model has a moderate consistency with samples R1 and R3, the value of χ being high but slightly lower than the average value and the modelled concentration being higher than the average value (Table 4). The model gives higher values against χ only with additional sample site (M6).

Monitoring data

The monitored daily average concentration time series for PM_{10} on the Turku air quality monitoring station (TMS) at city centre market square, Osiris 1 at Aninkaistenkatu (O1) city centre and Osiris 2 at Rakuunatie (O2) Vasaramäki city background show distinct differences in concentration levels between the locations (Fig. 5). Osiris 1 sensor at Aninkaistenkatu shows the highest concentrations whereas the Turku monitoring station exhibits much lower concentrations which are closer to the concentrations of Osiris 2 at Vasaramäki city background. The CAR-FMI modelled daily average PM_{10} concentrations follow a similar trend with the measured values; however, the difference in concentrations between locations is less prominent (Fig. 5). Furthermore, at site Osiris 1 the CAR-FMI modelled concentrations are clearly underestimated compared to the measured concentrations. The values of χ show a greater variability between locations than the CAR-FMI modelled concentrations, but they are still analogous with the measured daily average PM_{10} concentrations (Table 5), and this relation is emphasized by significant Spearman's rank correlation coefficient values of ($\rho = 1.000$, $p < 0.01$) between all the variables.

Statistical analysis

Spearman's rank order correlation coefficient at street level χ had a strong and significant correlation ($\rho = 0.679$–0.957, $p < 0.01$) with all the elements except Zn (Table 6). At street level, Fe had a strong and significant correlation ($\rho = 0.733$–0.955, $p < 0.01$) with all the elements, except only a moderate significant correlation ($p < 0.05$) with Zn and no significant correlation with Ba. However, with all street samples (St, M and R), both χ and Fe had strong and significant correlation ($p < 0.01$) with all the elements except Zn. Moreover, at roof level χ had a strong and significant correlation ($p < 0.01$) with elements Cu, Fe, Ti and a moderate correlation ($p < 0.05$) with Al, V and no correlation with Ba, Mn, Zn, Na, Ca and Mg. Furthermore, at roof level Fe had a strong and significant correlation ($p < 0.01$) with elements Al, Cu, Ti and a moderate correlation ($p < 0.05$) with Ba, V and no correlation with Mn, Zn, Na, Ca and Mg. Moreover, between χ and modelled PM_{10} concentrations there is no significant correlation at street level, whereas a moderate significant correlation at roof level ($\rho = 0.548$, $p < 0.05$). However, with all street samples (St, M and R) there is a significant moderate correlation ($\rho = 0.517$, $p < 0.01$) between χ and modelled PM_{10} concentrations (Table 6). Furthermore, a similar trend is shown between χ and annual average daily traffic flow (AADT), as there is no significant correlation with street (St) samples but a moderate significant correlation ($\rho = 0.557$, $p < 0.01$) with all street samples (St, M and

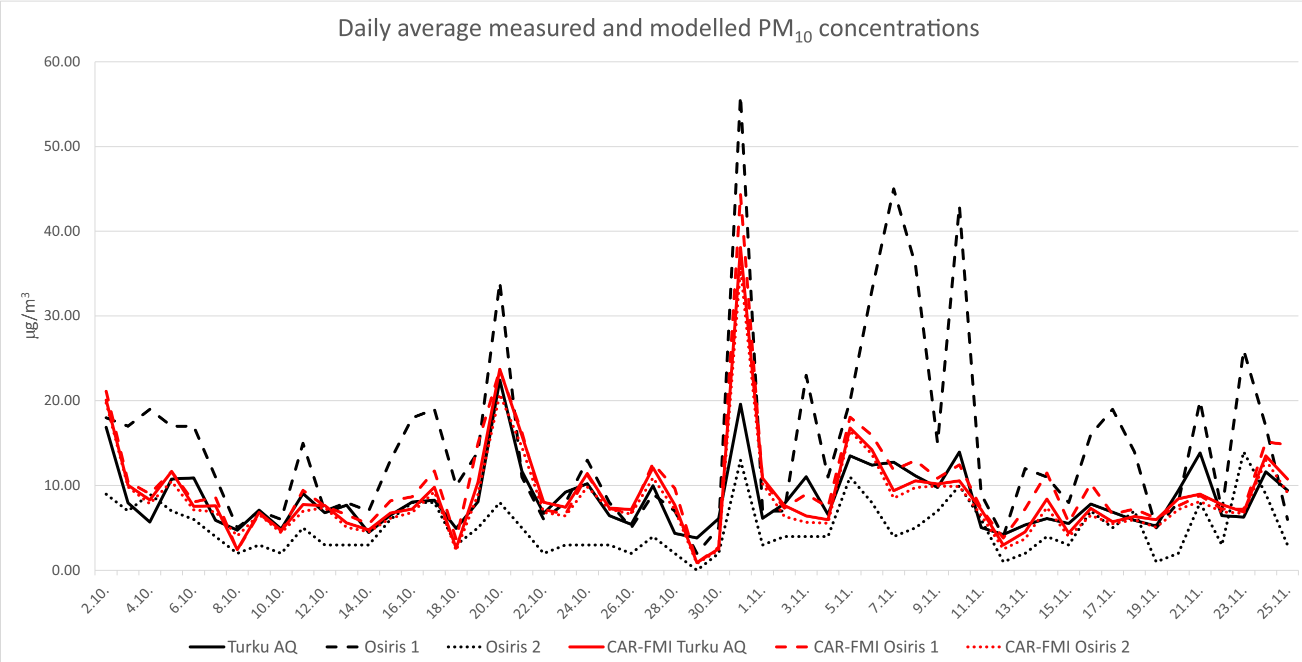

Fig. 5 Daily average measured and modelled concentrations of PM_{10} (µg/m^3) at Turku measuring station city centre, Osiris 1 at Aninkaistenkatu city centre and Osiris 2 at Rakuunatie Vasaramäki

Table 5 Average of daily PM_{10} concentrations (µg/m^3) for Turku measuring station (TMS), monitoring sensors (Osiris 1 and Osiris 2), mass-specific magnetic susceptibility (χ x $10^{-8}m^3kg^{-1}$) values and CAR-FMI modelled average of daily PM_{10} concentrations (µg/m^3) for same locations

	PM_{10}	χ	CAR-FMI PM_{10}
TMS/M7	8.53	4.05	9.02
Osiris 1	14.80	13.55	10.03
Osiris 2	5.00	0.85	8.33

R). The modelled $PM_{2.5}$ concentrations and χ have a weak significant correlation ($\rho = 0.475$, $p < 0.05$) only within all street samples (St, M and R).

Linear regression between χ and modelled PM_{10} concentrations shows a non-significant ($R^2 = 0.218$, $p = 0.79$, SEE = 0.82797) relationship with street (St) samples, a significant (R2 = 0.341, $p < 0.05$, SEE = 0.21797) relationship with roof (Rf) samples and a significant (R2 = 0.234, $p < 0.01$, SEE = 0.80014) relationship with all street (St, M, R) samples.

Mann-Whitney U-test showed significant differences in mass-specific magnetic susceptibility, element and modelled PM_{10} and $PM_{2.5}$ concentrations between street and roof level samples. The significant differences are shown with χ, Al, Cu, Fe, Mn, Ti, V, Na PM_{10} and $PM_{2.5}$ (Table 6). The elemental concentrations are exceptional, with Mn and Na as they have higher concentrations at roof level, whereas the other elements have higher concentrations at street level (Fig. 6).

In the principal component analysis (PCA), the Kaiser-Meyer-Olkin (KMO) value was 0.644 and Bartlett's test of sphericity $p = 0.001$ for street level and 0.624 and $p = 0.001$ for roof level, respectively. The PCA for elements in moss bags show two extracted factors for street level samples, which explain more than 84% of the total variance. The first factor explaining most of the variance (66%) with high loadings for Al, Ba, Cu, Fe, Mn, Ti, V, Ca and Mg and the second factor explains (18%) of the total variance with high loading for Zn (Table S4). The elements show three extracted factors for roof level samples, which explain more than 83% of the total variance (Table S5). The first factor explains (34%) of the variance with high loadings for Al, Cu, Fe and Ti, the second factor explains (33%) of the variance with high loadings for Ba, Zn, Ca and Mg and third factor explains (16%) of the variance with high loadings for V and Na.

The cluster analysis (CA) for the element variables in moss bags, are shown as dendrograms for street and roof level samples (Fig. 7). The dendrogram for elements at street level display two main clusters, where Zn is isolated into its own cluster. The second cluster seems to separate into two subclusters, where Ba, Fe, Cu are traffic-related and Na, Mn, Ca, V, Mg Ti, Al are more crustal and combustion-related. The dendrogram for elements at roof level display two main clusters, the first cluster including Ca, Ba, Mg, Zn, Mn and the second cluster including Na, V and Al, Cu, Ti, Fe. At roof level the source apportionment of the elements into clusters is more ambiguous.

Table 6 Summaries of Spearman's rank order correlation coefficient (n = 15) for mass-specific magnetic susceptibility (χ x $10^{-8}m^3kg^{-1}$), element concentrations (mg kg^{-1}), annual average daily traffic flow (AADT) and modelled average PM_{10} ($\mu g/m^3$) concentrations at street and roof level and all street samples, regression R^2 for mass-specific magnetic susceptibility (χ x $10^{-8}m^3kg^{-1}$) and modelled average PM_{10} ($\mu g/m^3$) concentrations at street and roof level and all street samples, Mann-Whitney U-test (MWU) to analyze significant differencies of mass-specific magnetic susceptibility, element and modelled average $PM_{2.5}$ and PM_{10} ($\mu g/m^3$) concentrations between street and roof level

	χ	Al	Ba	Cu	Fe	Mn	Ti	V
Street (St)								
ρ X	1.000	0.807**	0.713**	0.957**	0.893**	0.761**	0.812**	0.774**
ρ Fe	0.893**	0.929**	0.490	0.900**	1.000	0.844**	0.955**	0.733**
R^2 X								
Roof (Rf)								
ρ X	1.000	0.618*	0.446	0.947**	0.953**	0.024	0.894**	0.602*
ρ Fe	0.953**	0.740**	0.564*	0.937**	1.000	0.153	0.932**	0.594*
R^2 X								
Comparison (St & Rf)								
MWU	0.001	0.001	0.183	0.001	0.001	0.049	0.001	0.002
All Street (St, M, R)								
ρ X	1.000	0.785**	0.800**	0.978**	0.880**	0.787**	0.786**	0.828**
ρ Fe	0.880**	0.957**	0.776**	0.862**	1.000	0.873**	0.966**	0.889**
R^2 X								

	Zn	Na	Ca	Mg	AADT	CAR-FMI PM_{10}	CAR-FMI $PM_{2.5}$
Street (St)							
ρ X	0.557*	0.679**	0.730**	0.815**	0.496	0.286	0.236
ρ Fe	0.529*	0.742**	0.779**	0.941**	0.321	0.032	−0.110
R^2 X						0.218	
Roof (Rf)							
ρ X	0.158	0.481	0.350	0.108	0.592*	0.548*	0.517
ρ Fe	0.251	0.414	0.447	0.256	0.559*	0.443	0.410
R^2 X						0.341*	
Comparison (St & Rf)							
MWU	0.930	0.010	0.455	0.678		0.001	0.001
All Street (St, M, R)							
ρ X	0.368	0.752**	0.842**	0.788**	0.557**	0.517**	0.475*
ρ Fe	0.411	0.785**	0.904**	0.951**	0.457*	0.250	0.184
R^2 X						0.234**	

** Correlation/regression is significant at 0.01-level

* Correlation/regression is significant at 0.05-level

Discussion

Magnetic properties

The magnetic properties of traffic emission particulates are largely dominated by ferrimagnetic minerals such as magnetite (Sagnotti et al., 2009; Chaparro et al. 2020). Our results present narrow hysteresis loops and rapid saturations at 0.2–0.3 mT (Fig. 3) and low B_{CR} values (Table S3), suggesting the presence of low-coercivity ferrimagnetic minerals. Similar hysteresis curves and B_{CR} values were observed by Limo et al. (2024). The mean B_{CR} values 35.94, 36.86 and 36.99 mT for street (St), roof (Rf) and all street (St, M, R) samples fall well within the similar range described for anthropogenic magnetite (Sagnotti et al. 2006; Salo et al. 2012; Chaparro 2021) and traffic emissions (Gómez et al. 2021; Muxworthy et al. 2022; Chaparro et al. 2024), respectively. The concentration-dependent M_S and M_{RS} values (including χ values) fall within similar ranges as in other European cities (Szönyi et al. 2007; Winkler et al. 2020, 2022). Traffic-related magnetite has been the dominant low-coercivity ferrimagnetic mineral in previous air pollution-related moss bag studies in Turku (Salo and Mäkinen 2019; Limo et al. 2024), and according to the FMI (2022) air quality survey in the Turku region, the PM concentrations caused by industry or energy production are very low. Therefore, it is here plausible to assume that the predominant magnetic mineral in the moss bag samples is ferrimagnetic magnetite.

The positioning of the hysteresis ratios in the Day plot implies that they are most likely composed of a mixture of various magnetic grain sizes (Fig. 4). The mean B_{CR} values (35.94, 36.86 and 36.99 mT) might suggest broad grain-size distributions within PSD-stable SD-SP range (Limo et al. 2024). The domain states above the MD region suggest

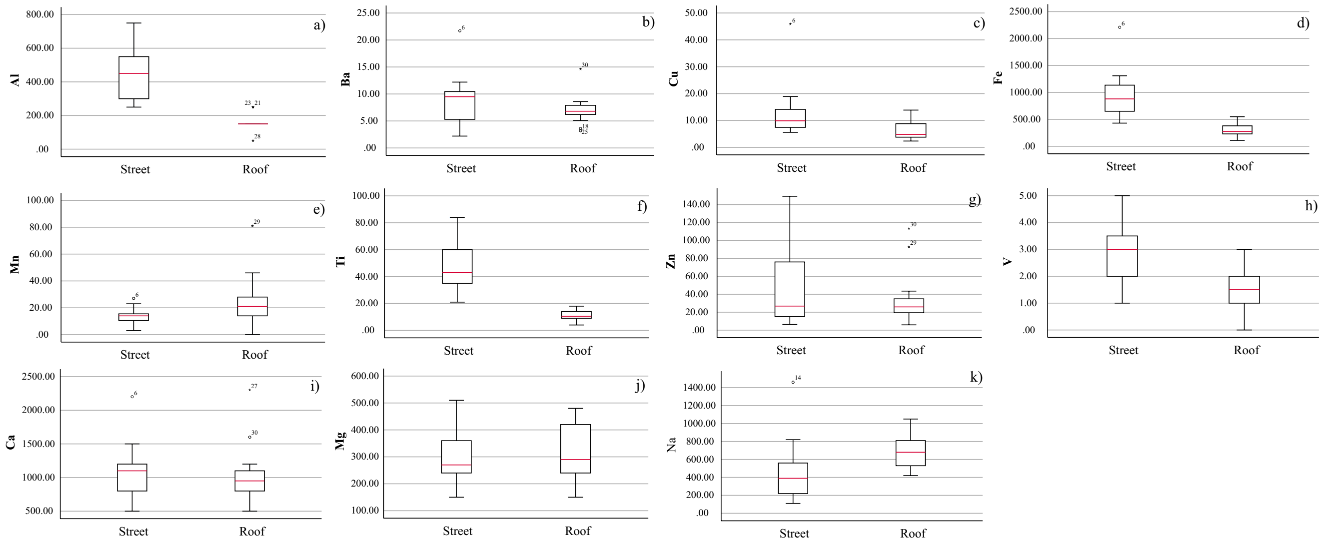

Fig. 6 Box plot diagrams of elements (mg kg^{-1}) on street and roof samples for (**a**) aluminium (Al), (**b**) barium (Ba), (**c**) copper (Cu), (**d**) iron (Fe), (**e**) manganese (Mn), (**f**) titanium (Ti), (**g**) zinc (Zn) and (**h**) vanadium (V), (**i**) calcium (Ca), (**j**) magnesium (Mg) and **k**) natrium (Na)

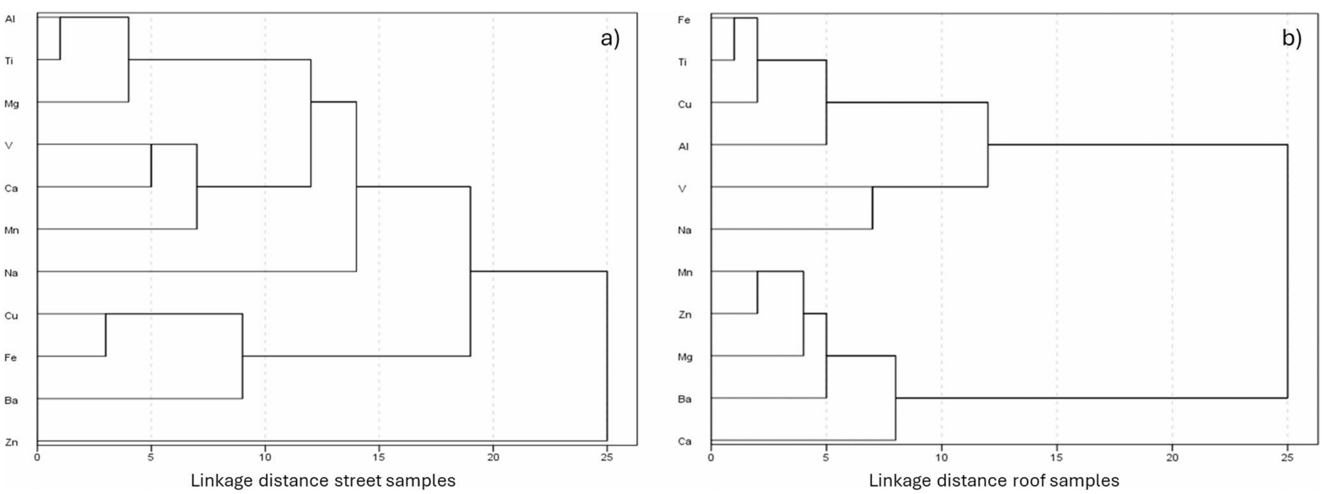

Fig. 7 Dendrograms from Ward's method of hierarchical cluster analysis of trace elements (**a**) street samples (**b**) roof samples. Diagrams representing hierarchical relationship between elements and showing how data is grouped into clusters based on similarity

grain-size differences within the magnetic PM, such as a mixture of PSD and MD with the presence of SP particles (Muxworthy at al., 2022). Magnetic PM is likely to be dominated by PM_{10}; however, grain sizes might suggest to a divided SP-PSD/MD distributions, where SP particles may be affiliated with traffic-related magnetic particles (Chaparro et al. 2020; Muxworthy et al. 2022). The SP grains may originate from traffic exhaust emissions and coarser fraction from abrasive wear of vehicle parts (Sagnotti et al. 2006), and according to Letaïef et al. (2024), our hysteresis ratios lie within the distributions represented by brake dust, mineral dust, street dust and gasoline particles. It is suggested that most of vehicle-traffic originated Fe-rich particles fall within $PM_{2.5}$ (Chaparro et al. 2020). Furthermore, it is estimated that up to 70% of airborne roadside magnetite originates from vehicle brake systems (Gonet et al. 2021). However, Tretiach et al. (2011) have emphasized that moss bags predominantly entrap fine particle ($<PM_{2.5}$) fraction over the coarse particle ($PM_{2.5–10}$) fraction. Moreover, Letaïef et al. (2024) conclude that passive sensors may always have a finer grain size distribution than the sources due to gravitational force, as finer grains travel further than coarse grains. Our hysteresis ratios show very similar SP-PSD/MD distributions to Muxworhty et al. (2022), but more importantly, they are in accordance with previous magnetic PM studies executed in Turku (Limo et al. 2018, 2024; Salo and Mäkinen 2019). The hysteresis ratios between street (St) and roof (Rf) samples show a slight shift towards to the PSD region. The positioning of grain sizes within the MD region has been related to increased accumulation of coarser

non-exhaust particles, especially to brake wear emissions, and finer exhaust emissions tend to settle more to the PSD region and even further to the linear trends of SD/MD mixtures (Winkler et al. 2022; Grifoni et al. 2025). This similar trend may be seen in the moss bag samples as the grain size distribution changes from coarse to finer within the magnetic PM due to the height difference between street and roof samples.

Elemental properties

The element abundance orders are identical between all street samples (St, M, R) and street samples (St), which strongly indicates a single dominant source for magnetic PM within the whole sample network. The element abundance orders in this study follow similar trends with previous studies carried out in Turku with only slight interchanges in the order position between Ti, Zn and Mn (Limo et al. 2018, 2024). Comparing street samples to roof samples, there is a distinct change in the element abundance order, as Na and Mg become the most abundant elements alongside with Ca. These elements are generally associated with crustal elements (Ca, Mg) and marine aerosols (Na) (Artíñano et al. 2004; Srimuruganandam and Shiva Nagendra 2011). With heavy metals, only Ti and Mn have interchanged their positions. The mean values for St and Rf samples show that for most of the heavy metals (Al, Ba, Cu, Fe, Ti, V and Zn) the roof concentrations decrease considerably, whereas the concentrations for Ca seem to remain rather stable between the different heights (Table 1). However, in the case of Mn, Na, Mg the concentration distributions between St and Rf samples appear to behave in an oppositely, as the highest concentrations of these elements are found on roof samples. It seems that with roof samples the crustal and marine elements become more abundant, and the concentrations of heavy metals seem to reduce. As crustal and marine related elements mainly occur in the coarse PM fraction ($PM_{2.5–10}$) and anthropogenic or traffic-related elements in the fine fraction ($PM_{2.5}$) (Hueglin et al. 2005; Srimuruganandam and Shiva Nagendra 2011), this might suggest that even fine particles associated with heavy metals are less likely to drift to upper layers of urban structures. According to Zhang et al. (2024) there is a decreasing trend with the abundance of traffic related magnetic PM in relation to height, and just below 29 m there is a zone dominated by ultrafine magnetic PM, an occurrence which might be apparent in roof samples Rf 2.1., 2.2., 2.3. and 3.1. However, in the case of Na, Ca and Mg only Na has a significant difference (*p*-value) with Mann-Whitney U test between the street and roof concentrations (Table 6). Eventually, this might indicate that at roof level long-distance transport is strongly influencing the concentrations of Na and also Ca and Mg, but with lower contribution.

The concentration of heavy metals Al, Ba, Cu, Fe, Ti, V and Zn relative to altitude seem to have a distinct drop in mean values as described above (Table 1), with the exception for Mn, which will be discussed later. Significant differences (*p*-value) between street and roof level concentrations are found in Al, Cu, Fe, Mn, Ti and V, which indicates that the quantity of traffic-related heavy metals is reduced at the top end of the urban canopy layer (Table 6). This tendency is also exhibited by the mass-specific magnetic susceptibility mean values (Table 1) and significant differences (*p*-value) (Table 6) between street and roof samples. As anthropogenic or traffic-related elements tend to occur in the fine fraction ($PM_{2.5}$) (Hueglin et al. 2005; Srimuruganandam and Shiva Nagendra 2011), it may suggest that fine particles and associated heavy metals mainly remain in the lower parts of the urban canopy as natural ventilation is reduced by complex urban structures. Therefore, suspension, resuspension and precipitation might be the most considerable factors determining concentrations of traffic-related magnetic PM and heavy metals on street level.

Distribution of heavy metal concentrations within the sample network is mainly concentrated on highly trafficked streets. The high values of χ usually reflect concentrations of elements, especially heavy metals (Al, Ba, Cu, Fe, Mn, Ti, V and Zn), but also crustal and marine elements (Ca, Mg and Na), and this tendency is observed in both street and roof samples (Tables 2, 3 and 4). The roof samples exhibit high values of χ and element concentrations mainly in connection with corresponding street sample sites. However, roof sample 3.1. is different as it has a higher value of χ than the corresponding street sample along with high concentrations of the other elements. This sample site is rather close to the train station (ca. 150 m south), but it is difficult to determine how the train traffic could influence on element concentrations. In the case of city background samples, CBN shows higher concentrations of χ and other elements than CBS. This could be interpreted as pollution transport from the city centre but is most likely caused by the heavy traffic from the Naantali highway. Since city background sample sites in east (CBE) and west (CBW) were badly damaged, the interpretation of remaining two city background sample sites in contrast to the city roof sample sites was omitted.

An interesting anomaly uprises with manganese as it has the highest concentrations at roof level almost throughout the whole sample network (Tables 2 and 3). The high concentrations of manganese seem to be analogous with traffic volume, but very high concentrations are found close to the harbour at roof sample sites Rf 4.1., 4.2., (5.1) and (5.2) The exhausts from ship traffic is released at higher altitudes, but whether the high overall concentrations of Mn throughout the sample network are caused by this or by traffic cannot be assessed reliably in this study. However, automobile and ship traffic are found to be a source for outdoor urban Mn pollution (Finkelstein and Jerret, 2007; Zhao et al. 2013).

Mass-specific magnetic susceptibility (χ) and Fe have significant correlations with all the other elements at street level, suggesting that magnetic PM and iron are highly associated with the abundance of the other elements (Table 6). The same tendency is not so obvious at roof level as χ correlates significantly only with Al, Cu, Fe, Ti and V and iron with Al, Ba, Cu, Ti and V. For Fe and Ba however, there is a peculiarity with correlations between street (St) and all street (St, M and R) samples as there is no correlation with the former and a strong significant correlation with the latter. As Ba is regarded as a trace element for brake wear (Winkler et al. 2022), it seems that with more sample sites situated in the city centre trafficked areas, a stronger relation between Fe and Ba arises. It may indicate that the street (St) sample sites are less influenced by traffic intensity or stop-and-go traffic. Nevertheless, the strong interaction with χ, Fe and the other elements at street level strongly suggests that traffic is the main source for the pollution. The park and river sample sites illustrate low values of χ and element concentrations. This exemplifies how magnetic PM is associated with traffic and the vicinity of the source, and distance to the source is reflected by a drop in values. On the other hand, there is a strong correlation between χ and Fe with Al which indicates extensive crustal (soil and road wear) resuspension loading in the magnetic PM, mainly at street level but extending to roof level as well. At roof level, the overall concentrations of magnetic PM and related elements from street traffic may have decreased relevantly, and long-distance transport may also influence the observed outcome.

The principal component analysis (PCA) also points to a single source of pollution for street samples, as only two factors are extracted, and the first factor includes most of the elements Al, Ba, Cu, Fe, Mn, Ti, V, Ca and Mg, explaining 66% of the total variance (Table S4). Only Zn is allocated to the second factor, and Na not belonging to either of the two factors. A similar tendency is shown in the cluster analysis (CA) for street samples, illustrating only two major clusters with Zn and rest of the elements. It seems that in the second cluster two groups are connected at some distance, the more traffic related Cu, Fe and Ba and the slightly more crustal origin related Al, Ti, Mg, V, Ca, Mn and Na (Fig. 7). The peculiar behaviour of Zn within the magnetic PM is also noticeable in previous studies performed in the Turku urban area (Limo et al. 2018, 2024). Zn has been generally used as a tire wear particle tracer, but this has been debated in recent studies (Alves et al. 2020; Chen et al. 2023). However, the affiliation between zinc and χ or Fe has previously occurred as a weak or no correlation (Limo et al. 2018, 2024), and similar results are observed in this study as well (Table 6). This may imply that somehow Zn is not involved in the similar speciation process with magnetic Fe particulates and therefore behaves differently from the rest of the elements within the magnetic PM.

Interestingly, heavy metal concentration studies of soils in Turku by Salonen and Korkka-Niemi (2007) suggest that the concentration of Zn in topsoil (0–5 cm) varies between 4 and 499 mg/kg (median 73.80 mg/kg) and is controlled by variations in anthropogenic pollution. In our moss bag samples at street level, the concentration of Zn varies between 0.7 and 405.80 mg/kg, and the median values of sample sets between 12.15 and 26.80 mg/kg (Table 1). The highest values, exceeding the threshold limit of 200 mg/kg for soil contamination, were found from sites M1 (405.80 mg/kg) right next to a large playground area and Park 1 (228.50 mg/kg) with three nearby playgrounds with sandy surfaces. The exposed fill-up soils and highly turbulent wind conditions in these locations might explain the higher Zn values in moss bags. At the roof level, the highest Zn values in the moss bags are clearly found within the harbour area (samples Rf 5.1. and Rf 5.2.) which is located ca. 5 km to SE of the Meyer Turku shipyard.

On the other hand, the PCA for roof samples exhibits a more diverse outcome as three factors are extracted. The first factor includes Al, Cu, Fe and Ti, the second factor Ba, Mn, Zn, Ca and Mg, and the third factor V and Na with total variance percentages of 34%, 33% and 16%, respectively (Table S5). The CA for roof samples shows two main clusters connected with distance and the first cluster is again dividing into two separate clusters. The second cluster is mainly composed of elements (Mn, Zn, Mg and Ca), which do not correlate with either χ or Fe (Table 6), apart from Ba which has a weak correlation only with iron. Within the first cluster, the elements (Fe, Ti, Cu, Al and V) have strong correlation with χ and iron, except with Na, which does not correlate at all with either. This might suggest that the second cluster is slightly more affected by long-distance transport and the first cluster with traffic-related particles from lower altitudes, or there might be some form of coupling happening within the magnetic PM as altitude increases and distance to the original source is increased.

Air quality modelling

CAR-FMI modelling was applied for street and roof level to estimate the dispersion of PM against the accumulated magnetic PM (χ) throughout the sample network (Tables 2, 3 and 4). With street (St) level samples, there is no significant correlation ($\rho = 0.286$) between the magnetic PM and modelled PM; however, there seems to be some consistency with concentrations, as high or low values correspond to each other (Table 2). There are significant moderate correlations between χ and modelled PM_{10} with roof (Rf) ($\rho = 0.548$, $p < 0.05$) and all street (St, M and R) ($\rho = 0.517$, $p < 0.01$) level samples (Table 6). The linear regression between χ and modelled PM resembles the correlations, as there is a non-significant relationship with street (St) samples and a significant relationship with all street (St, M, R) samples ($R^2 = 0.234$) and roof (Rf) samples ($R^2 = 0.341$). Even though, there is a statistical discrepancy in correlations between street (St) and all street (St, M, R) samples in relation to modelled PM, the M and R samples resemble similar consistency with concentrations to street (St) samples, as high or low values seem to correspond to each other (Tables 2 and 4). This similar consistency with corresponding high and low values is not so evident with the roof samples, as more of the modelled PM values tend to be higher than the related magnetic PM values (Table 3).

In addition, there is a peculiar correlation between χ and modelled PM_{10}, which is identical to Fe and Ba discussed earlier. With street (St) and all street (St, M and R) samples, there is no correlation with the former and a significant moderate correlation with the latter. Similar to Fe and Ba, the correlation between χ and modelled PM_{10} seems to arise when more sample sites situated in the city centre trafficked areas are added. Thereby, traffic intensity seems to have a significant influence on the relation between χ and $PM_{10,}$ as also observed by Winkler et al. (2021), and as emphasized by the moderate significant correlation between χ and annual average daily traffic flow (AADT).

Nevertheless, the model produces a few clear exceptions of street samples with higher concentrations estimates (St 1.2., St 3.1. and M 6) and lower concentration estimates (St 5.1. and St 5.2.) at some of the street sample sites. The locations where the model gives higher PM concentrations in contrast to magnetic PM are street sections with high traffic densities. It may be that the values of χ are low because of local circumstances that influence the accumulation magnetic PM in the moss bags, like, for example, vicinity of small local park areas (St 3.1. and M 6) and topographic disturbance from a close by hill (St 1.2.). The lower PM concentration estimations in comparison with magnetic PM at St (5.1) and St (5.2) might be related to the vicinity of the harbour and traffic congestion at these sample sites during on-and-off vehicle traffic to ferryboats. The CAR-FMI model calculations did not include the traffic to ferryboats. Furthermore, according to Srimath et al. (2017), the modelling does not sufficiently include the increased emissions during traffic congestion. It may also be that the emissions from the ferryboat traffic have an influence on the accumulation of magnetic PM at the sample sites, as they are located upwind to the general wind directions from the harbour (Fig. 1). In the case of St 1.3., St 3.3., St 4.1., R1 and R3 the model estimations and the χ values are slightly different, but quite close to the mean value, so it is secure to interpret that they are analogous.

In the case of the roof (Rf) samples, the modelled PM concentrations seem to correspond accordingly with the high magnetic PM values at sample sites 2.1., 2.2., 2.3. and 3.1., and the low magnetic PM values at sample sites 1.1., 4.3., (5.1) and (5.2) Only at roof sample 4.2. the modelled PM concentrations underestimate the magnetic PM values. With street and roof samples 2.1., 2.2. and 2.3. the modelled and magnetic PM values are unison, which indicates that in these locations the model estimates well how the particles from street are drifted to the roof level. However, in contrast to magnetic PM, the model overestimates PM concentrations at roof sites 1.2., 1.3., 3.2., 3.3. and 4.1. On the other hand, the model estimates for roof level PM concentrations are mostly higher than estimates based on magnetic PM measurements. This may simply reflect the fact that the roof level and street level PM composition and magnetic PM content are different. However, this might also reflect the fact that CAR-FMI is a gaussian plume model, which does not really understand the built environment and the resulting complicated vertical/3D velocity fields, which very easily may lead to overestimation at roof level.

Air quality monitoring

Air quality monitoring stations produce valuable data, and they are usually used for monitoring assessment thresholds for regulated pollutants with reference measurement methods. The sampling points for reference monitoring stations are sited in such a way that provides data from areas with the highest concentrations (hotspots) where population is likely to be exposed and in more remote areas (urban or rural background) that represent the exposure of the general population (EU, 2024). Sampling points should also be representative of similar locations not in their immediate vicinity, i.e. how the measuring data reflects the air quality over a larger area. Therefore, the spatial representativeness is utter most important criterion for monitoring station placement, as it is crucial for the critical assessment in contrast to air quality standards and exposure to pollution concentration (EU, 2024). In Turku, the air quality monitoring station (TMS) is situated in the city centre marketplace (Fig. 1), which might not be the most representative traffic site location to measure exposure to concentrations of traffic-related air pollution. The assessment of representativeness of TMS was conducted by placing additional moss bags samples (R1, R2, R3, R4, Park 1 and Osiris 1) in the urban environment surrounding the city marketplace. A reference moss bag sample M7 was placed at the marketplace to reflect magnetic PM concentrations in the vicinity of the TMS. The

Table 7 Mass-specific magnetic susceptibilities (χ x $10^{-8}m^3kg^{-1}$) and element concentrations (mg kg^{-1}) at locations surrounding the Turku monitoring station (TMS) to assess representativeness

	M7/TMS	Park 1	R1	R2	R3	R4	Osiris 1	Osiris 2	Average (R1-4, O1)	Median (St, M, *R*)
Χ	4.05	3.50	11.10	2.98	10.85	25.45	13.55	0.85	12.79	10.43
Al	150	150	150	150	150	350	250	50	210	350
Ba	3.70	2.00	3.90	0.20	3.40	10.20	6.40	5.10	4.82	6.00
Cu	5.10	3.25	10.46	5.25	9.63	21.06	10.96	1.28	11.47	9.35
Fe	260	200	480	190	490	950	620	80	546	705
Mn	2.00	3.00	5.00	0.00	7.00	16.00	11.00	15.00	7.80	11.00
Ti	11	8	18	8	18	38	25	3	21.40	34.00
V	1	0	1	0	2	4	2	0	1.80	2.00
Zn	5.3	228.5	18.8	22.6	0.7	46.7	5.9	22.6	18.94	20.85
Na	110	340	340	20	30	740	100	50	246	280
Ca	500	400	700	300	600	1400	700	300	740	800
Mg	100	110	120	50	90	330	180	90	154.0	240

Sample site M7 represents Turku monitoring station

Samples sites (M) are located in the middle of the cell created by the street and roof samples and samples sites (R) are located around the Turku marketplace to assist in evaluating representativeness of Turku monitoring station, (O) are the Osiris sensor sample sites

mass-specific magnetic susceptibility values χ and metals are evidently lower at site M7 than in the surrounding R1, R3, R4 or Osiris 1 and resemble concentrations more relative to sample site Park 1 (Table 7). This may arise from the circumstance that the marketplace is an open area and traffic surrounding it is partly restricted only to buses and taxis, and this may result in a misleading representativeness of a sample point. Furthermore, at site M7 the concentrations of χ and all elements are lower than the average of the representative traffic samples (R1-4 and Osiris 1) and the median values of all street samples (St, M, R) (Table 7). Importantly, the daily average PM concentrations of the two Osiris monitoring sensors agree with the moss bag magnetic PM measurements and the CAR-FMI modelled PM concentrations (Table 5). However, at site Osiris 1 the CAR-FMI model clearly underestimates concentrations and this might be caused by a street canyon effect (Limo et al. 2024). The highest daily average PM concentrations (Fig. 5) and the concentrations of χ and the elements (Table 7) are found at site Osiris 1, second highest at TMS/M7 and the lowest values at Osiris 2. In relation to Salo and Mäkinen (2019), our results also suggest that the monitoring station at Turku marketplace may underestimate PM levels. Instead of proposing to remove a monitoring station with a valuable long series of air quality measurements, it is here suggested that a serious consideration and inspection should take place to evaluate if the monitoring station should be recategorized as a city background station.

Moss bag technique

Our study reinforces the excellence of the moss bag technique as a powerful tool in magnetic biomonitoring of urban airborne pollution. It enables a plethora of approaches for studying the distributions of PM within the complex urban architecture and offers a great spatial resolution with long sampling periods. Not only does it create the opportunity to study PM in various dimensions, but it also allows a unique possibility for assessing the representativeness of monitoring stations and the performance of air quality models. The method serves as a valuable and cost-effective tool to study the distributions and concentrations of PM pollution from a variety of sources and environments.

Conclusions

Examination of the urban canopy layer with moss bags and magnetic measurements demonstrate that traffic is the most significant source of low-coercivity ferrimagnetic minerals and heavy metals in the ambient urban street environment. The magnetic PM is comprised of magnetite and a mixture of PSD/MD grains with the presence of SP particles. At higher altitudes, the concentrations of magnetic PM and traffic-related elements are reduced and mainly replaced with crustal elements and are most likely influenced by long-distance transport. There is a significant moderate correlation between the CAR-FMI model and magnetic PM concentrations at roof level, but no correlation with corresponding street level samples. With a larger number of street samples, there is a significant moderate correlation between modelled PM concentrations and magnetic PM. At roof level, the CAR-FMI modelled PM concentrations are prone to overestimation compared to values indicated by the magnetic PM measurements. The magnetic measurement values correspond strongly with the data from the Turku monitoring station and monitoring sensors installed for this study. It is suggested that the representativeness of the Turku monitoring station should be reconsidered, and recategorizing may be appropriate. Magnetic biomonitoring using moss bags is a multipurpose tool for studying airborne pollution in the urban canopy layer and a reliable instrument for assessing monitoring stations and dispersion model performance.

Supplementary Information The online version contains supplementary material available at https://doi.org/10.1007/s11869-026-02059-5.

Acknowledgements This study was funded by the Finnish Cultural Foundation (grants 00160572, 00170629 and 00180659) and the Department of Geography and Geology, University of Turku. We would like to thank all the housing cooperatives and the housing landlords who gave us the permission to utilize their property for the roof sampling. We would like to thank Turku infrastructure services for allowing us to use city property for the street sampling. In addition, we would like to thank Turku public authority Miika Meretoja for assistance, Daniela Hellgren for assistance with GIS and Camilla Gustafsson for comments on the manuscript.

Authors' contributions Jukka Limo – Conceptualization, Methodology, Formal analysis, Investigation, Writing original draft, Data curation, Visualization, Project administration and Funding acquisition. Mari Kauhaniemi – Methodology, Software, Validation, Formal analysis, Resources, Data curation, and Writing review & editing. Leena Kangas - Methodology, Software, Validation, Formal analysis, Resources, Data curation, and Writing review & editing. Petriina Paturi – Methodology, Software, Formal analysis, Resources and Data curation and Writing review & editing. Joni Mäkinen – Conceptualization, Resources, Writing review & editing and Supervision. Ari Karppinen – Conceptualization, Resources, Writing review & editing and Supervision.

Funding Open Access funding provided by University of Turku (including Turku University Central Hospital). This study was funded by the Finnish Cultural Foundation (grants 00160572, 00170629 and 00180659).

Data availability The datasets generated during and/or analysed during the current study are available from the corresponding author on reasonable request.

Declarations

Ethics approval and consent to participate Not applicable.

Consent for publishing All authors consent to the publication of this study.

Competing interests The authors have no relevant financial or non-financial interests to disclose.

References

Aarnio MA, Kukkonen J, Kangas L, Kauhaniemi M, Kousa A, Hendriks C, Yli-Tuomi T, Lanki T, Hoek G, Brunekreef B, Elolähde T, Karppinen A (2016) Modelling of particulate matter concentrations and source contributions in the Helsinki Metropolitan Area in 2008 and 2010. Boreal Environ Res 21(5–6):445–460. http://hdl.handle.net/10138/225788

Alves CA, Vicente AMP, Calvo AI, Baumgardner D, Amato F, Querol X, Pio C, Gustafsson M (2020) Physical and chemical properties of non-exhaust particles generated from wear between pavements and tyres. Atmos Environ 224:117252. https://doi.org/10.1016/j.atmosenv.2019.117252

Artíñano B, Salvador P, Alonso DG, Querol X, Alastuey A (2004) Influence of traffic on the PM_{10} and $PM_{2.5}$ urban aerosol fractions in Madrid (Spain). Sci Total Environ 334–335, pp. 111–123. https://doi.org/10.1016/j.scitotenv.2004.04.032

Beddows DCS, Harrison RM (2021) PM_{10} and $PM_{2.5}$ emission factors for non-exhaust particles from road vehicles: Dependence upon vehicle mass and implications for battery electric vehicles. Atmos Environ 244:117886. https://doi.org/10.1016/j.atmosenv.2020.117886

Castañeda-Miranda AG, Chaparro MAE, Pacheco-Castro A, Chaparro MAE, Böhnel HN (2020) Magnetic biomonitoring of atmospheric dust using tree leaves of *Ficus benjamina* in Querétaro (México). Environ Monit Assess 192:382. https://doi.org/10.1007/s10661-020-8238-x

Chaparro MAE, Chaparro MAE, Castañeda-Miranda AG, Marié DC, Garguilo JD, La-vornia JM, Natal M, Böhnel HN (2020) Fine air pollution particles trapped by street tree barks: In situ magnetic biomonitoring. Environ Pollut 266:115229. https://doi.org/10.1016/j.envpol.2020.115229

Chaparro MAE (2021) Airborne particle accumulation and loss in pollution-tolerant lichens and its magnetic quantification. Environ Pollut 288:117807. https://doi.org/10.1016/j.envpol.2021.117807

Chaparro MAE, Posada DB, Chaparro MAE, Molinari D, Chiavarino L, Alba B, Marié DC, Natal M, Böhnel HN, Vaira M (2024) Urban and suburban's airborne magnetic particles accumulated on *Tillandsia capillaris*. Sci Total Environ 907:167890. https://doi.org/10.1016/j.scitotenv.2023.167890

Chen L-W, Antony, Wang X, Lopez B, Wu G, Ho SSH, Chow JC, Watson JG, Yao Q, Yoon S, Jung H (2023) Contribution of non-tailpipe emission to near-road $PM_{2.5}$ and PM_{10}: A chemical mass balance study. Environ Pollut 335:122283. https://doi.org/10.1016/j.envpol.2023.122283

Cristaldi A, Fiore M, Conti GO, Pulvirenti E, Favara C, Grasso A, Copat C, Ferrante M (2022) Possible association between $PM_{2.5}$ and neurodegenerative diseases: A systematic review. Environ Res 208:112581. https://doi.org/10.1016/j.envres.2021.112581

Dunlop DJ (2002) Theory and application of the Day plot (M_{rs}/M_s versus H_{cr}/H_c) 2. Application to data for rocks, sediments, and soils. J Geophys Res. https://doi.org/10.1029/2001JB000487

Dunlop DJ (2021) Magnetic hysteresis of magnetite at high temperature: grain size variation. Geophys J Int 225:816–827. https://doi.org/10.1093/gji/ggab138

Eckhardt J (2019a) Suomen tieliikenteen päästöt ja energiankäyttö kunnittain vuonna 2017, VTT LIISA laskentajärjestelmä,

kunnat2017.xlsx, Päivitetty 24.1.2019, http://lipasto.vtt.fi/liisa/kunnat.htm, downloaded 8.8.2024.
Eckhardt J (2019b) Suomen tieliikenteen päästöt ja energiankäyttö kunnittain vuonna 2017, VTT LIISA laskentajärjestelmä, kunnat2018.xlsx, Päivitetty 21.8.2019. http://lipasto.vtt.fi/liisa/kunnat.htm, downloaded 8.8.2024
European Institute of Innovation and Technology Urban Mobility (EIT Urban Mobility) (2025) Study on non-exhaust emissions in road transport. https://www.eiturbanmobility.eu/wp-content/uploads/2025/05/41-EIT-Emissions-Report-5a-Digital-1.pdf
European Environment Agency (EEA) (2019) The European environment — state and outlook 2020: Knowledge for transition to a sustainable Europe. Eur Environ Agency. https://doi.org/10.2800/96749
European Environment Agency (EEA) (2022) Managing air quality in Europe, Publications Office of the European Union, 2022. https://data.europa.eu/doi/10.2800/851688
European Environment Agency (EEA) (2023) Europe's air quality status 2023, Publications Office of the European Union. EEA Briefings 5/2023, https://data.europa.eu/doi/10.2800/59526
European Union (EU) (2024) Directive (EU) 2024/2881 of the European Parliament and of the Council of 23 October 2024 on ambient air quality and cleaner air for Europe. https://eur-lex.europa.eu/eli/dir/2024/2881/oj
Finkelstein MM, Jerret M (2007) A study of the relationships between Parkinson's disease and markers of traffic-derived and environmental manganese air pollution in two Canadian cities. Environ Res 104:420–432. https://doi.org/10.1016/j.envres.2007.03.002
Finnish Meteorological Institute (FMI) (2020) Jatta Salmi, Emmi Laukkanen, Timo Rasila, Hanna Hannuniemi, Birgitta Komppula, Katja Lovén. The Air quality survey in Turku region. FMI expert services – Air quality and energy (in Finnish). https://expo.fmi.fi/aqes/public/Turun_seudun_ilmanlaatuselvitys_2020.pdf
FMI (2024) The Finnish Meteorological Institute's open data. https://en.ilmatieteenlaitos.fi/opendata, downloaded 1.11.2024.
Finnish Standards Association SFS (1994) Air protection. Bioindication. Moss bag method. Stand-ard SFS 5794 (in Finnish). http://www.sfs.fi/en
Gómez RQ, Chaparro MAE, Chaparro MAE, Castañeda -Miranda AG, Marié DC, Gar-guilo JD, Böhnel HN (2021) Magnetic biomonitoring using native Lichens: Spatial distribution of traffic-derived particles. Water Air Soil Pollution 232:124. https://doi.org/10.1007/s11270-021-05047-w
Gonet T, Maher BA, Kukutschová J (2021) Source apportionment of magnetite particles in roadside airborne particulate matter. Sci Total Environ 752:141828. https://doi.org/10.1016/j.scitotenv.2020.141828
Grifoni L, Winkler A, Chaparro MAE, Di Lella LA, Marte F, Sgamellotti A, Spagnuolo L, Tascon M, Buitagro Posada F, Marié DC, Scoccimarro M, Loppi S (2025) Magnetic and chemical biomonitoring with lichens and vascular plants for the preservation of cultural heritage: A case study at two museums in a megacity (Buenos Aires, Argentina). Sci Total Environ 988:179836. https://doi.org/10.1016/j.scitotenv.2025.179836
Gustafsson M (2018) Chapter 8 - Review of Road Wear Emissions. A review of road wear emission measurement studies: Identification of gaps and future needs. In: Amato F (ed) Non-Exhaust Emissions, An urban Air quality Problem for Public Health. Academic Press, pp 161–182. https://doi.org/10.1016/B978-0-12-811770-5.00008-X
Hansard R, Maher BA, Kinnersley R (2011) Biomagnetic monitoring of industry derived particulate pollution. Environ Pollut 159(6):1673–1681. https://doi.org/10.1016/j.envpol.2011.02.039
Hofman J, Samson R (2014) Biomagnetic monitoring as a validation tool for local air quality models: a case study for an urban street canyon. Environ Int 70:50–61. https://doi.org/10.1016/j.envint.2014.05.007
Hueglin C, Gehrig R, Baltensperger U, Monn G, Vonmont C H (2005) Chemical characterisation of $PM_{2.5}$, PM_{10} and coarse particles at urban, near-city and rural sites. Atmos Environ 39:637–651. https://doi.org/10.1016/j.atmosenv.2004.10.027
Härkönen J (2002) Regulatory dispersion modelling of traffic-originated pollution. Academic Dissertation in physics. Finnish Meteorological Institute Contributions No. 38, ISSN 0782–6117. https://helda.helsinki.fi/server/api/core/bitstreams/cc324986-fb29-4940-b8fc-24bbd338ef38/content
Jackson M, Worm H-U, Banerjee SK (1990) Fourier analysis of digital hysteresis data: rock magnetic applications. Phys Earth Planet Inter 65:78–87. https://doi.org/10.1016/0031-9201(90)90077-B
Järlskog I, Jaramillo-Vogel D, Rausch J, Gustafsson M, Strömvall A-M, Andersson-Sköld Y (2022) Concentrations of tire wear microplastics and other traffic-derived non-exhaust particles in the road environment. Environ Int 170:107618. https://doi.org/10.1016/j.envint.2022.107618
Karppinen A, Joffre SM, Kukkonen J (2000) The refinement of a meteorological preprocessor for the urban environment. Int J Environ Pollut 14:565–572. https://doi.org/10.1504/IJEP.2000.000580
Kauhaniemi M, Karppinen A, Härkönen J, Kousa A, Alaviippola B, Koskentalo T, Aarnio P, Elolähde T, Kukkonen J (2008) Evaluation of a modelling system for predicting the concentrations of $PM_{2.5}$ in an urban area. Atmos Environ 42:4517–4529. https://doi.org/10.1016/j.atmosenv.2008.01.071
Kauhaniemi M, Kukkonen J, Härkönen J, Nikmo J, Kangas L, Omstedt G, Ketzel M, Kousa A, Haakana M, Karppinen A (2011) Evaluation of a road dust suspension model for predicting the concentrations of PM10 in a street canyon. Atmos Environ 45:3646–3654. https://doi.org/10.1016/j.atmosenv.2011.04.055
Ketzel M, Omstedt G, Johansson C, Düring I, Pohjola M, Oettl D, Gidhagen L, Wåhlin P, Lohmeyer A, Haakana M, Berkowicz R (2007) Estimation and validation of $PM_{2.5}$/PM_{10} exhaust and non-exhaust emission factors for practical street pollution modelling. Atmos Environ 41:9370–9385. https://doi.org/10.1016/j.atmosenv.2007.09.005
Kim T-Y, Kim H, Yi S-M, Cheong J-P, Heo J (2018) Short-term effects of ambient $PM_{2.5}$ and $PM_{2.5–10}$ on mortality in major cities of Korea. Aerosol Air Qual Res 18:1853–1862. https://doi.org/10.4209/aaqr.2017.11.0490
Kupiainen K (2007) Road dust from pavement wear and traction sanding. Monographs of the Boreal Environment Research 26, 52. Finnish Environment Institute
Lahti J, Sainio P (2021) Road Traffic Act reform: impact on the use of winter and summer tyres, The Finnish Transport and Communications Agency Traficom, Traficom Research Reports 10/2021, 26.10.2021, p. 37. ISSN 2669–8781
Lazić L, Aničić Urošević M, Mijić Z, Vuković G, Ilić L (2016) Traffic contribution to air pollu-tion in urban street canyons: Integrated application of the OSPM, moss biomonitoring and spectral analysis. Atmos Environ 141:347–360. https://doi-org.ezproxy.utu.fi/https://doi.org/10.1016/j.atmosenv.2016.07.008
Letaïef S, Carvallo C, Franke C, Isambert A, Camps P (2024) Contributions and limitations of environmental magnetism to characterize traffic-related particulate matter sources. Geophys J Int vol 237(3):1505–1525. https://doi.org/10.1093/gji/ggae108
Li C, Liu M, Hu Y, Wang H, Xiong Z, Wu W, Liu C, Zhang C, Du Y (2022) Investigating the vertical distribution patterns of urban air pollution based on unmanned aerial vehicle gradient monitoring. Sustainable Cities Soc 86:104144. https://doi.org/10.1016/j.scs.2022.104144
Limo J, Paturi P, Mäkinen J (2018) Magnetic biomonitoring with moss bags to assess stop-and-go traffic induced particulate matter and

heavy metal concentration. Atmos Environ 195:187–195. https://doi.org/10.1016/j.atmosenv.2018.09.062
Limo J, Kauhaniemi M, Paturi P, Keskinen J-P, Karppinen A, Mäkinen J (2024) Another one bites the dust – Two street canyons studied with magnetic biomonitoring and OSPM modelling. Atmos Environ 319:120312. https://doi.org/10.1016/j.atmosenv.2023.120312
Mathias AD, Comrie AC, Musil SA (2006) Atmospheric pollution. In: Pepper IL, Gerba CP, Brusseau ML (eds) Environmental and Pollution Science. Academic Press Inc., USA, pp 377–394
Matzka J, Maher BA (1999) Magnetic biomonitoring of roadside tree leaves: identification of spatial and temporal variations in vehicle-derived particulates. Atmos Environ 33:4565–4569. https://doi.org/10.1016/S1352-2310(99)00229-0
Muxworthy AR, Lam C, Green D, Cowan A, Maher BA, Gonet T (2022) Magnetic characteri-sation of London's airborne nanoparticulate matter. Atmosph Environ 287:119292. https://doi.org/10.1016/j.atmosenv.2022.119292
Mäkelä K, Auvinen H (2009) LIPASTO – transport emission database, in: Life cycle assessment of products and technologies, VTT Symposium 262, VTT, Vuorimiehentie, pp. 134–142
Omstedt G, Bringfelt B, Johansson C (2005) A model for vehicle-induced non-tailpipe emissions of particles along Swedish roads. Atmosph Environ 39:6088–6097. https://doi.org/10.1016/j.atmosenv.2005.06.037
Panko J, Kreider M, Unice K (2018) Chapter 7 - Review of tire wear Emissions. A review of tire emission measurement studies: Identification of gaps and future needs. In: Amato F (ed) Non-Exhaust Emissions, An Urban Air Quality Problem for Public Health. Academic Press, pp 147–160. https://doi.org/10.1016/B978-0-12-811770-5.00007-8
Paoli L, Winkler A, Guttová A, Sagnotti L, Grassi A, Lackovičová A, Senko D, Loppi S (2017) Magnetic properties and element concentration in lichens exposed to airborne pollutants released during cement production. Environ Sci Pollut Res Int 24(13):12063–12080. https://doi.org/10.1007/s11356-016-6203-6
Potter NA, Meltzer GY, Avenbuan ON, Raja A, Zelikoff JT (2021) Particulate matter and associated metals: a link with neurotoxicity and mental health. Atmosphere (Basel) 12(4):425. https://doi.org/10.3390/atmos12040425
REDUST (2014) Demonstration test final report: Main results and conclusions, Deliverable product of the REDUST LIFEC project Actions 1 and 2. http://www.ymk-projektit.fi/redust//files/2015/02/REDUST-Action-1-2-final-report.pdf, last access: 15 October 2014
Sagnotti L, Macri P, Eglli R, Mondino M (2006) Magnetic properties of atmospheric particulate matter from automatic air sampler stations in Latium (Italy): Toward a definition of magnetic fingerprints for natural and anthropogenic PM_{10} sources. J Phys Res 111:B12S22 https://doi.org/10.1029/2006JB004508.
Sagnottti L, Taddeucci J, Winkler A, Cavallo A (2009) Compositional, morphological, and hysteresis characterization of magnetic airborne particulate matter in Rome, Italy. Geochem Geophys Geosyst 10:8. https://doi.org/10.1029/2009GC002563
Salo H, Bućko M, Vaahtovuo E, Limo J, Mäkinen J, Pesonen L (2012) Biomonitoring of air pollution in SW Finland by magnetic and chemical measurements of moss bags and lichens. J Geochem Explor 115:69–81. https://doi.org/10.1016/j.gexplo.2012.02.009
Salo H, Mäkinen J (2019) Comparison of traditional moss bags and synthetic fabric bags in magnetic monitoring of urban air pollution. Ecol Indic 104:559–566. https://doi.org/10.1016/j.ecolind.2019.05.033
Salonen V-P, Korkka-Niemi K (2007) Influence of parent sediments on the concentration of heavy metals in urban and suburban soils in Turku, Finland. Appl Geochem 22:906–918. https://doi.org/10.1016/j.apgeochem.2007.02.003
Srimath STG, Sokhi R, Karppinen A, Singh V, Kukkonen J (2017) Evaluation of an urban modelling system against three measurement campaigns in London and Birmingham. Atmospheric Pollution Res 8:38–55. https://doi.org/10.1016/j.apr.2016.07.004
Srimuruganandam B, Shiva Nagendra SM (2011) Chemical characterization of PM_{10} and $PM_{2.5}$ mass concentrations emitted by heterogeneous traffic. Sci Total Environ 409:3144–3157. https://doi.org/10.1016/j.scitotenv.2011.04.042
Soares J, Plass D, Kienzler S, González Ortiz A, Gsella A, Horálek J (2023) Health Risk Assessment of Air Pollution: assessing the environmental burden of disease in Europe in 2021 (Eionet Report – ETC HE 2023/7). European Topic Centre on Human Health and the Environment. https://www.ccacoalition.org/resources/health-risk-assessment-air-pollution-assessing-environmental-burden-disease-europe-2021
Szönyi M, Sagnotti L, Hirt AM (2007) On leaf magnetic homogeneity in particulate matter biomonitoring studies. Geophys Res Lett. https://doi.org/10.1029/2006GL029076
Tretiach M, Pittao E, Crisafulli P, Adamo P (2011) Influence of exposure sites on trace element enrichment in moss-bags and characterization of particles deposited on the biomonitor surface. Sci Total Environ 409:822–830. https://doi.org/10.1016/j.scitotenv.2010.10.026
Turku (2017) Turun kaupunkiseudun ilmanlaatu vuonna 2017, Turun seudun ilmansuojelun yhteistyöryhmä, https://www.naantali.fi/sites/default/files/media/file/Vuosiraportti%202017%20kannellinen.pdf
Turku region air protection collaboration group (2021) Turku region air quality in 2021 (in Finnish). https://www.naantali.fi/sites/default/files/media/file/Turun%20kaupunkiseudun%20ilmanlaadun%20vuosiraportti%202021.pdf
Vuković G, Aničić Urošević M, Goryainova Z, Pergal M, Škrivanj S, Samson R, Popović A (2015) Active moss biomonitoring for extensive screening of urban air pollution: Magnetic and chemical analyses. Sci Total Environ 521–522:200–210. https://doi.org/10.1016/j.scitotenv.2015.03.085
Wahlström J, Olander L, Olofsson U (2010) Size, shape and elemental composition of airborne wear particles from disc brake materials. Tribol Lett 38:15–24
Winkler A, Contardo T, Vannini A, Sorbo S, Basile A, Loppi S (2020) Magnetic emission from brake wear are the major source of airborne particulate matter bioaccumulated by lichens. Appl Sci 10:2073. https://doi.org/10.3390/app10062073
Winkler A, Amoroso A, Di Giosa A, Marchegiani G (2021) The effect of Covid-19 lockdown on airborne particulate matter in Rome, Italy: a magnetic point of view. Environ Pollut 291:118191. https://doi.org/10.1016/j.envpol.2021.118191
Winkler A, Contardo T, Lapenta V, Sgamellotti A, Loppi S (2022) Assessing the impact of vehicular particulate matter on cultural heritage by magnetic biomonitoring at Villa Farnesina in Rome, Italy. Sci Total Environ 823:153729. https://doi.org/10.1016/j.scitotenv.2022.153729
World Health Organization (WHO) (2021) Air Quality Guidelines - Update 2021. WHO Reg Office Europe. https://iris.who.int/server/api/core/bitstreams/551b515e-2a32-4e1a-a58c-cdaecd395b19/content. Copenhagen, Denmark
Xin K, Zhao J, Ma X, Han L, Liu Y, Zhang J, Gao Y (2021) Effect of urban underlying surface on PM2.5 vertical distribution based on UAV in Xi'an, China. Environ Monit Assess 193(5):312. https://doi.org/10.1007/s10661-021-09044-8
Yang T, Liu Q, Li H, Zeng Q, Chan L (2010) Anthropogenic magnetic particles and heavy metals in the road dust: Magnetic identification and its implications. Atmos Environ 44:1175–1185. https://doi.org/10.1016/j.atmosenv.2009.12.028
Zhang R, Li M, Wu D, Ren X, Wang Z, Ou Y (2024) Vertical variation in magnetic particles within atmospheric PM in indoor dustfall

in industrial cities of northern China. Atmospheric Pollut Res 15:102075. https://doi.org/10.1016/j.apr.2024.102075
Zhao M, Zhang Y, Ma W, Fu Q, Yang X, Li C, Zhou B, Yu Q, Chen L (2013) Characteristics and ship traffic source identification of air pollutants in China's largest port. Atmos Environ 64:277–286. https://doi.org/10.1016/j.atmosenv.2012.10.007